BIT Numerical Mathematics (2025) 65:46
https://doi.org/10.1007/s10543-025-01088-3

BIT

The numerical linear algebra of weights. Part I: from the spectral analysis to conditioning and preconditioning in the one-dimensional Laplacian case

Ludovico Bruni Bruno[1,2] · **Matteo Semplice**[3] · **Stefano Serra-Capizzano**[3,4]

Received: 3 February 2025 / Accepted: 20 October 2025

Abstract

Weights are geometrical degrees of freedom that allow to generalize Lagrangian finite elements. They are defined through integrals over specific supports, well understood in terms of differential forms and integration, and lie within the framework of finite element exterior calculus. We adopt this formalism with the target of identifying supports that are appealing for a finite element approximation, describing weights in terms of a single parameter in the third- and fourth-order methods. To do so, we study the related parametric matrix-sequences, with the matrix order tending to infinity as the mesh size tends to zero. Using the generalized locally Toeplitz theory, we analyze the performance of weights-based finite elements on an elliptic operator. In particular, for degrees 3 and 4, we identify an optimal value for the weights location, which sits in a rather large interval where weights give rise to better conditioned stiffness matrices. With this at hand, we propose and test ad hoc preconditioners, in dependence of the discretization parameters and in connection with conjugate gradient method. The model problem we consider is a one-dimensional Laplacian, both with constant and non-constant coefficients. Numerical visualizations and experimental tests are reported and critically discussed, showing a confidence interval for the choice of the parameter.

✉ Ludovico Bruni Bruno
ludovico.brunibruno@unipd.it

Matteo Semplice
matteo.semplice@uninsubria.it

Stefano Serra-Capizzano
s.serracapizzano@uninsubria.it

1 Dipartimento di Matematica "Tullio Levi-Civita", Università di Padova, Padua, Italia

2 Istituto Nazionale di Alta Matematica, Francesco Severi, Roma, Italia

3 Dipartimento di Scienza e Alta Tecnologia, Università dell'Insubria, Como, Italia

4 Department of Information Technology, Division of Scientific Computing, Uppsala University, Uppsala, Sweden

Published online: 05 November 2025

Keywords Exterior calculus · Finite elements · Weight selection · Spectral distribution of matrix-sequences · Conditioning · Preconditioning

Mathematics Subject Classification 15A18 · 65N30 · 47B35 · 65F10 · 65F08

1 Introduction

Discretizations of (differential) operators usually yield very large linear systems. Performing valuable spectral analyses of their matrices is thus an important step in the construction of many numerical methods [35, 36, 46, 52]. These analyses can also be used to select optimal parameters. For instance, they have been deployed to investigate stabilization parameters and CFL numbers both in the one-dimensional [47] and multi-dimensional [48] hyperbolic framework. We are here concerned with the detection of well conditioned bases (compatibly with the structure of the operator) for the finite elements method (FEM) [31].

In its essence, a FEM is specified by a triangulation $\mathcal{T}$ of the domain Ω, a finite dimensional space X where the solution is sought, and a set of linear functionals on X named *degrees of freedom* (*dofs*). The triangulation $\mathcal{T}$ contains the *elements* and approximates Ω with respect to an appropriate measure. Functions in X have small support, so the matrix A of the system, which represents the bilinear form associated with a weak formulation of the problem, is sparse and often sparse in a d-level sense if $\Omega \subset \mathbb{R}^d$ [52]. The role of dofs is then twofold: they determine a basis for X by duality and prescribe gluing conditions between local solutions on neighbouring elements. The dofs we consider in this paper are named *weights* [53, 54], and are designed to capture the geometrical and physical features of the problem [19].

When the space X consists of functions, weights can be represented as nodal evaluations. If such points are equidistributed in the element, one retrieves usual Lagrange elements, which can be consequently regarded as a particular case of weights-based elements. Furthermore, if $\dim \Omega = 1$, continuous weights-based elements have a dof located at each endpoint of any element, whereas the other dofs shall be placed inside each interval of the mesh $\mathcal{T}$.

While the choice of the space X controls the Galerkin approximation error, the choice of a basis $\{\varphi_i\}_{i=1}^N$ for X heavily affects the conditioning of the matrix A; this is discussed in Section 4 and visualized in Figure 5. Hence this choice is as important as the approximation features, for mostly three reasons:

- the inherent error depends on the condition number and this is independent of the method – either direct or iterative – used for solving the resulting linear system;
- the speed of convergence of an iterative solver is directly affected by the conditioning, in a way depending often on the method itself;
- a convenient choice of basis may make it easier to construct an effective preconditioner for A.

The conditioning of A is not the only actor for understanding the convergence speed of (preconditioned) Krylov solvers in the Hermitian positive definite setting. The global distribution of the eigenvalues plays a crucial role in the (preconditioned)

conjugate gradients (see [15, 42]). This applies also to the MINRES, for Hermitian possibly indefinite (preconditioned) matrices, or to GMRES for (preconditioned) normal matrices. For the latter, in the general setting, the eigenvalues do not describe completely the convergence history and more information is needed, involving either the field of values or the conditioning of the eigenvector matrix, when the (preconditioned) coefficient matrix is diagonalizable; see, e.g., [17, 40, 45]. In Section 5 in fact we observe that an incorrect selection of the location parameter representing the dofs yields both an increment of the conditioning and a spreading of the spectrum of the preconditioned matrix.

In this work we develop a general theory and specialize it to the analysis of the role of dofs location in a one-dimensional context. This simplification is advantageous under the two following points of view: first, the notation can be kept plain, and second, the generalized locally Toeplitz (GLT) machinery may be applied to a one-parameter family of weights-based continous FEM. In turn, we obtain a class of theoretical results that extend well known spectral features of usual equidistributed Lagrangian finite elements, which are in fact retrieved for a specific choice of the parameter. An interesting aspect emerges in the computational analysis of the parameter: there is a confidence interval where the conditioning of the matrix of the system is lower than that of usual Lagrangian elements, with only one global minimum. This leads to a proposal for the weights' location that minimizes the conditioning of A. This is computationally cheap, as GLT theory ensures that the optimal value is independent of the number of elements used in the discretization, as this optimization is performed through the analysis of an $r \times r$ matrix for a FEM of degree r. This peculiarity also persists in more involved situations, for instance in the presence of non-constant coefficients and non-uniform grids. Although this analysis is targeted at different objects from those usually considered in weights-based interpolation theory [6, 20, 22], it is worth pointing out that optimality and quasi-optimality results emerging from both these streams of research fall close to each other.

Furthermore, we exploit the study of the spectrum of A to develop a circulant GLT-based preconditioner, whose performance turns out to be stable not only in such interval, but also for parameters that are sufficiently close to such an interval. In contrast, a rough distribution of the weights not only makes the conditioning grow uncontrollably, but also implies a spread in the spectrum of the preconditioned matrices. An undesirable effect of this is a reduction of the speed of convergence of the iterative method.

Outline of the paper. The paper is organized as follows. In Section 2 we introduce the formalism of finite element exterior calculus (FEEC), the corresponding bases, the notion of weights-based dofs, their duality and the weak formulation of the test cases. This part is general, and paves the way for non standard nodal degrees of freedom and multi-dimensional applications. Section 3 is devoted to the derivation of the spectral symbol and the key spectral characteristics of weights-based FEM. We here specialize to the one-dimensional setting and recover general results in such a framework. To make the analysis more concrete, in Section 4, we specify degrees 3 and 4. These cases are associated with a one-parameter family of GLT sequences: we carry an explicit spectral analysis and the consequent optimization, focusing also on a preconditioning

strategy. Visualizations of theoretical findings and numerical experiments are given in Section 5. Finally, in Section 6, we gather conclusions and indicate future lines of research opened by our investigation. For completeness, Appendix A contains a short account on the main aspects of GLT theory. This part, which contains well established definitions and results, is omitted from the main part of the paper for readability.

2 Weights-based FEM

Finite element exterior calculus [10] is a modern approach to the numerical solution of differential problems. It enforces the domain topology into the discretization, avoiding many pitfalls related to the appearance of spurious numerical modes, and summarizes a wide class of operators in a single formulation involving an operator acting on differential forms [1, 28]. It is in the spirit of this generality that in this section we present the formulation of the Hodge Laplacian, the generalization of the Laplacian operator acting on differential forms. Later on we specialize to the well known one-dimensional Laplace operator acting on functions. Performing the analysis of its discretization within this larger setting puts us in the position to provide some general claims that are useful in later analysis for the broader class of Laplace operators.

In the framework of FEEC, shape functions are thought of as differential forms $\Lambda^k(\Omega)$ [68], namely sections of the k-th exterior power of the cotangent bundle of Ω [1]. Thus, 0- and n-forms (with $n = \dim \Omega$) are functions, 1- and $(n-1)$-forms are (dual to) vector fields, and so on. An overview of possible local spaces, together with their assembled counterparts, is offered in the *Periodic Table of finite elements* [11]. Among them, we recall Lagrangian elements, Nédélec elements, Raviart-Thomas elements, and discontinuous elements.

Regardless of the local basis, the construction of the bases for the FEM discretization space is generally performed using the so-called affinely equivalent elements; see [27, Chapter 2.3] and [31, Chapter 9] for a classical introduction or [41] and [44] for a FEEC-oriented approach.

Fix a reference element $\widehat{T}$ and a vector space $\widehat{\mathcal{P}} \subset \Lambda^k(\widehat{T})$ of k-forms defined on $\widehat{T}$. For any element $T_i \in \mathcal{T}$, let $\psi_i : T_i \to \widehat{T}$ be an invertible affine map such that $\psi_i(T_i) = \widehat{T}$. It induces a pullback

$$\psi_i^* : \quad \Lambda^k(\widehat{T}) \to \Lambda^k(T_i)$$

which preserves polynomial objects [10, 20]. The coordinate representation of the pullback depends on k: it reads as composition for nodal elements, Piola (covariant and contravariant) mappings for vector fields, and so on. As a consequence, the choice of $\widehat{\mathcal{P}}$ induces a space of forms $\mathcal{P}_i$ defined on T_i and basis on $\widehat{T}$ induces a basis of $\mathcal{P}_i$. The FEM space X is a space of forms defined on $\bigcup_{T_i \in \mathcal{T}} T_i$ such that their restriction to any element T_i belongs to $\mathcal{P}_i$.

Bases in duality. Let $\{\mathrm{dof}_i : \widehat{\mathcal{P}} \to \mathbb{R}\}_{i=1}^{N_{\mathrm{loc}}}$ be a collection of linear functionals that form a basis of the dual space of $\widehat{\mathcal{P}}$, where $\dim \widehat{\mathcal{P}} = N_{\mathrm{loc}}$. These degrees of freedom

induce a basis $\{\omega_i\}_{i=1}^{N_{\text{loc}}}$ on $\widehat{\mathcal{P}}$, such that

$$\text{dof}_i(\widehat{\omega}_j) = \delta_{i,j}.$$

When mappings dof_i are *moments* [10, 49, 50] or *weights* [53, 54], these bases are not explicitly known, apart from few cases. Nevertheless, if $\{\widehat{\varphi}_i\}_{i=1}^{N_{\text{loc}}}$ is any *convenient* basis, one may consider the *generalized Vandermonde matrix* [31] V, defined as

$$V_{i,j} \doteq \text{dof}_i(\widehat{\varphi}_j), \tag{1}$$

in order to obtain an explicit expression for the dual basis [20]. Since $\{\widehat{\omega}_i\}_{i=1}^{N_{\text{loc}}}$ and $\{\widehat{\varphi}_i\}_{i=1}^{N_{\text{loc}}}$ are bases for the same vector space $\widehat{\mathcal{P}}$, they are related as

$$\widehat{\omega}_i = \sum_{j=1}^{N_{\text{loc}}} W_{i,j}\widehat{\varphi}_i, \tag{2}$$

where the matrix W is invertible. Then

$$V_{i,j} = \text{dof}_i(\widehat{\varphi}_j) = \text{dof}_i\left(\sum_{k=1}^{N} W^{-1}_{j,k}\widehat{\omega}_k\right) = \sum_{k=1}^{N} W^{-1}_{j,k}\text{dof}_i(\widehat{\omega}_k) = W^{-1}_{j,i} = W^{-T}_{i,j}$$

and, as a consequence,

$$W = V^{-T}. \tag{3}$$

2.1 Weights

A natural operation on differential forms is *integration*: a differential k-form can be integrated over a k-dimensional manifold. This suggests the introduction of *weights* [19, 53, 54] as degrees of freedom.

Definition 1 Let ω be a smooth k-form and let s be a k-simplex. The weight of ω over s is

$$w(\omega, s) \doteq \int_s \omega. \tag{4}$$

Remark 1 In the literature, the normalized (through the measure of s) version of (4) is equally diffused. Such two definitions coincide in the nodal case $k = 0$, as the measure of a point is assumed to be 1. For $k > 0$ they present some subtle differences, even in the one-dimensional framework. This problem is addressed, for instance, in [23]. We elaborate on this in further detail in Section 2.2.

Weights provide meaningful degrees of freedom for any finite dimensional space of polynomial differential forms $\widehat{\mathcal{P}}$ (and therefore for any $\mathcal{P}_k$) as long as the generalized

Vandermonde matrix (1) is square and invertible, see, e.g., [4, 5]. Notice that, in this case, the (i, j)-th element of this matrix is simply

$$V_{i,j} = w(\omega_j, s_i) = \int_{s_i} \omega_j, \tag{5}$$

being $\{s_i\}_{i=1}^{N_{\text{loc}}}$ a collection of $N_{\text{loc}} = \dim \widehat{\mathcal{P}}$ k-simplices supported in $\widehat{T}$. Any set $\{s_i\}_{i=1}^{N_{loc}}$ such that $\det V_{i,j} \neq 0$ is said to be *unisolvent* for the space $\widehat{\mathcal{P}}$. The search for unisolvent sets is, in general, a tough problem, which has only partial theoretical solutions in the case of simplicial elements [20, 24]. The projector induced by weights is usually studied in literature [22] via the *generalized Lebesgue constant* [8].

Weights for polynomial differential forms have the same scope of other degrees of freedom, such as moments; nevertheless, they have a geometrically strong characterization and hence allow for localization techniques [7]. Explicit applications of weights-based FEM may be found in [9, 53].

The Hodge Laplacian. Consider the differential problem on $\Lambda^k(\Omega)$ given by

$$\begin{cases} -L\omega = f, \\ \text{boundary conditions on } \omega\big|_{\partial\Omega}. \end{cases} \tag{6}$$

Given two smooth functions $b, c : \Omega \to \mathbb{R}$, we define $L : \Lambda^k(\Omega) \to \Lambda^k(\Omega)$ as

$$L = b\mathrm{d}c\mathrm{d}^* + c\mathrm{d}^*b\mathrm{d}.$$

If $b = c = 1$ this operator is the usual Hodge Laplacian [68]

$$\Delta_H : \quad \omega \mapsto \left(\mathrm{d}\mathrm{d}^* + \mathrm{d}^*\mathrm{d}\right)\omega,$$

whose role in PDEs is largely described in [56]. A weak formulation for (6) is obtained by introducing the L^2-inner product on differential forms

$$(\omega, \eta)_2 \doteq \int_\Omega \omega \wedge \star\eta, \tag{7}$$

see [43]. The operator $\star$ is the Hodge star isomorphism [68]. Stokes' Theorem

$$\int_\Omega \mathrm{d}\omega = \int_{\partial\Omega} \omega$$

and Leibniz' rule lead to the following integration by parts formula

$$\int_\Omega \mathrm{d}\omega \wedge \eta = (-1)^{k-1} \int_\Omega \omega \wedge \mathrm{d}\eta + \int_{\partial\Omega} \omega\big|_{\partial\Omega} \wedge \eta\big|_{\partial\Omega}, \tag{8}$$

which prescribes the boundary conditions to turn the first equation of (6) into the *Poisson problem for differential forms*. For $c = 1$, imposing $\omega\big|_{\partial\Omega} = 0$ and exploiting (8), we deduce the weak formulation

$$(b\mathrm{dd}^*\omega, \eta)_2 + (\mathrm{d}^* b\mathrm{d}\omega, \eta)_2 = (f, \eta)_2 \quad \forall \eta \in \Lambda^k(\Omega). \tag{9}$$

When $d = 1$ either the first or the second term of the above left hand side vanish. For $k = 0$, where $(b\mathrm{dd}^*\omega, \eta)_2 = 0$, one obtains the bilinear form

$$a(\omega, \eta) \doteq \int_I b\mathrm{d}\omega \wedge \star\mathrm{d}\eta.$$

Identifying 0-forms with functions, it is immediate to acknowledge that this is the counterpart of the elliptic problem with diffusion coefficient $b(x)$:

$$\int_I b(x)u'(x)v'(x)\mathrm{d}x = \int_I f(x)v(x)\mathrm{d}x, \quad u\big|_{\partial I} = 0. \tag{10}$$

For $k = 1$, weights are expressed as (possibly normalized) line integrals over segments supported in $I = \Omega$. In this case one has $(\mathrm{d}^* b\mathrm{d}\omega, \eta)_2 = 0$, and a further idetification via the Hodge star operator is needed to retrieve the bilinear form (10). The situation becomes more involved, for instance allowing for discretizations based on discontinuous elements. A discussion on the topic in expanded in Section 2.2.

The stiffness matrix. Given a basis $\{\varphi_i\}_{i=1}^N$ for X, a FEM Galerkin approach for the approximation of (10) leads to the linear system $A\widetilde{u} = F$, with A being the *stiffness* matrix

$$A_{i,j} = a(\varphi_i, \varphi_j) = \int_I b(x)\varphi_i'(x)\varphi_j'(x)\mathrm{d}x \tag{11}$$

and F the column vector with entries

$$F_i = \int_I f(x)\varphi_i(x)\mathrm{d}x.$$

Clearly the solution $\widetilde{u}$ does not depend on the choice of the basis functions φ_i's, but it is now explicit that the features of the matrix A do.

Our analysis exploits the assembly procedure from local matrices, which is as follows. Consider a basis for X which is dual to a collection of $N = \dim(X)$ dofs together with a "local to global" mapping

$$\mathrm{LTG}: \quad \{1, \dots, N_{\mathrm{loc}}\} \times \mathcal{T} \to \{1, \dots, N\}$$

and the assumption that the global $\mathrm{dof}_{\mathrm{LTG}(i,k)}$ coincides with the local dof_i when applied to the pullback of forms in $\mathcal{P}_k$. Therefore the restriction of the global basis functions satisfies

$$\forall i \in \{1, \dots, N_{\mathrm{loc}}\}\ \forall T_k \in \mathcal{T}: \quad \varphi_{\mathrm{LTG}(i,k)}\big|_{T_k} = \phi_k^* \left(\widehat{\omega}_i\right).$$

Then, for any element $T_k \in \mathcal{T}$, one introduces the local matrices by restricting the integrals in the weak formulation to one specific element T_k and changing variables to perform integration on the reference element as

$$A_{i,j}^{(T_k)} = \int_{\widehat{T}} b(\psi_k(\hat{x}))\widehat{\omega}_i'(\hat{x})\widehat{\omega}_j'(\hat{x})\mathrm{d}\hat{x}. \tag{12}$$

The global stiffness matrix can then be assembled as

$$A = \sum_{T_k \in \mathcal{T}} \sum_{i=1}^{N_{\mathrm{loc}}} \sum_{j=1}^{N_{\mathrm{loc}}} \mathrm{E}_{\mathrm{LTG}(i,k),\,\mathrm{LTG}(j,k)} \left(A_{i,j}^{(T_k)} \right),$$

where $\mathrm{E}_{i,j}(x)$ is an $N \times N$ matrix with only one nonzero entry, equal to x, at location (i, j). This yields the following description of the matrix of the system.

Proposition 1 *Let A and B be the stiffness matrices written with respect to the bases $\{\varphi_i\}_{i=1}^N$ and respectively $\{\omega_i\}_{i=1}^N$; there exists an invertible matrix M such that*

$$A = M^{-T} B M^{-1}. \tag{13}$$

Moreover, the elemental matrices $A^{(T_k)}$ and $B^{(T_k)}$ for $T_k \in \mathcal{T}$ written with respect to $\{\widehat{\varphi}_i\}_{i=1}^{N_{loc}}$ and respectively to $\{\widehat{\omega}_i\}_{i=1}^{N_{loc}}$, satisfy

$$A^{(T_k)} = V^{-T} B^{(T_k)} V^{-1}. \tag{14}$$

Proof Equality (13) is a general fact of linear algebra. Equality (14) is a direct consequence of (12) and (3), being $\{\widehat{\varphi}_i\}_{i=1}^{N_{loc}}$ the basis in duality with the degrees of freedom. □

Remark 2 Equation (14) mixes ingredients of very different nature: matrices $A^{(T_k)}$ and $B^{(T_k)}$ are local and depend on the bilinear form a, see Eq. (12). In contrast, the generalized Vandermonde matrix does not depend on a, see Eq. (5), and is *global* in the following sense. Let $V^{(T_k)}$ be the generalized Vandermonde matrix relating the two local bases $\{\psi^*(\widehat{\varphi}_i)\}$ and $\{\psi^*(\widehat{\omega}_i)\}$ on the element T_k. With reference to Eq. (5), one has

$$V_{i,j}^{(T_k)} = \int_{\psi_k^{-1}(s_i)} \psi_k^*(\widehat{\omega}_j) = \int_{s_i} \widehat{\omega}_j = V_{i,j}.$$

Remark 3 Notice that, in general, the matrix M in (13) may be intricate to compute. In contrast, the Vandermonde matrix given in Eq. (1) is usually easy to handle, as described in [3]. The relationship (14) then allows to work with a convenient basis on the reference element and to compute the local matrices during assembly.

This approach is particularly useful when basis functions associated with a set of local dofs are not known in explicit form, for instance in the multivariate framework; see [52] for a two-dimensional account.

We make use of such a result for the segmental case $k = 1$.

Remark 4 It is well known that too naive Vandermonde matrices, such as those associated with the monomial basis and nodes on the real line, are inherently exponentially ill-conditioned as a function of the matrix order [61]. Although this turns into a tangible problem for mild to large polynomial degrees [64], this aspect is not secondary and should be taken into consideration, for instance employing comparably easy to handle but better conditioned bases. An example is the Bernstein basis; a comparison between Vandermonde matrices associated with the monomial and the Bernstein bases can be found in [20, Tables 3.1 and 3.2].

2.2 The case $k = 1$: the histopolation problem

When $k = 1$, the term $(\mathrm{d}^* b \mathrm{d}\omega, \eta)_2$ in Eq. (9) vanishes due to dimensional reasons. The remaining term requires the projection onto a space of (discrete) differential 1-forms. These operators are known as *histopolators* [55], and replace the usual nodal interpolation conditions for a function f with either

$$\int_{s_i} p(x)\mathrm{d}x = \int_{s_i} f(x)\mathrm{d}x, \qquad i = 1, \dots, N_{\mathrm{loc}}, \tag{15}$$

or their normalized variant (also referred to as "interpolation of cell averages" in the literature of finite volume schemes [69])

$$\frac{1}{|s_i|}\int_{s_i} p(x)\mathrm{d}x = \frac{1}{|s_i|}\int_{s_i} f(x)\mathrm{d}x, \qquad i = 1, \dots, N_{\mathrm{loc}}. \tag{16}$$

In the above equations, s_i represents a segment contained in I. Upon some natural assumptions, such as the disjointedness (in measure) of the supports s_i, these conditions are clearly equivalent to interpolation conditions on some *unknown* nodes $\xi_i \in s_i$, $i = 1, \dots, N_{\mathrm{loc}}$, via the mean value theorem. This gives the following localization result for the zeros of such polynomials; see [23, Proposition 1].

Lemma 1 *Suppose supports* $\{s_i\}_{i=1}^{N_{\mathrm{loc}}}$ *are disjoint. Then there exists a unique polynomial* $p(x)$ *of degree* $N_{\mathrm{loc}} - 1$ *that satisfies* (15) *and* (16). *Further, if* $\{\varphi_j\}_{j=1}^{N_{\mathrm{loc}}}$ *is the cardinal basis satisfying*

$$\frac{1}{|s_i|}\int_{s_i} \varphi_j(x)\mathrm{d}x = \delta_{i,j},$$

then $\varphi_j(x)$ *has exactly one zero in the interior of each* s_i, *for* $i \neq j$, *and* $\varphi_j(x) > 0$ *for each* $x \in s_j$.

Lagrange bases associated with (15) and (16) scale accordingly to the normalization factor [23, Eq. (14)] only when the measures $|s_i|$ are bounded away from zero for each i. In such a case, Lemma 1 implies that discretizations based upon degrees of freedom as in (15) immediately lead to discontinuous elements. The discontinuous case requires a careful choice of stabilization parameters [25].

In contrast, interelement continuity can be enforced also in this framework considering (16) in place of (15) and allowing segments s_i to shrink to single points ξ_i.

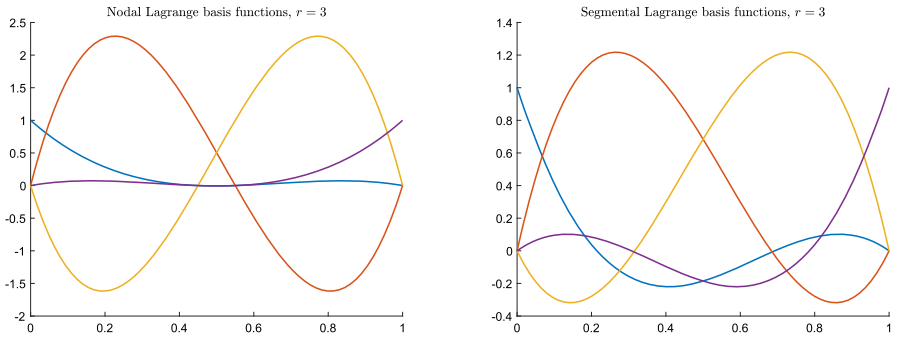

Fig. 1 Nodal Lagrange bases (left) and segmental Lagrange bases (right) for $\xi = 0.45$. The case depicted is $r = 3$

An immediate continuity argument, together with the mean value theorem, implies that one falls again into continuous elements as long as this is imposed on the first and the last segment. While the space spanned by the corresponding Lagrange polynomials is still the same, such functions are in essence different from the usual ones obtained for the nodal case $k = 0$, due to the non-constructiveness of the mean value theorem. An instance of this follows from the next result, which we state on $[-1, 1]$ only for notational simplicity. The extension to any other segment of the real line is straightforwardly obtained by composing with an appropriate affine map.

Proposition 2 *Let $\{s_i\}_{i=1}^{N_{\mathrm{loc}}}$ be disjoint segments in I, and let $\{\varphi_i\}_{i=1}^{N_{\mathrm{loc}}}$ be the corresponding Lagrange basis with respect to (16). Suppose the set $\{s_i\}_{i=1}^{N_{\mathrm{loc}}}$ is symmetric with respect to 0, meaning that if $s_i = [\eta_i, \gamma_i]$ then $s_{N_{\mathrm{loc}}+1-i} = [-\gamma_i, -\eta_i]$. Then, for each $i = 1, \dots, N_{\mathrm{loc}}$,*

$$\varphi_i(x) = \varphi_{N_{\mathrm{loc}}+1-i}(-x).$$

Proof The disjointedness of the segments grants unisolvence, hence the existence of the cardinal basis $\{\varphi_i\}_{i=1}^{N_{\mathrm{loc}}}$. Observing that symmetry implies $|s_i| = |s_{N_{\mathrm{loc}}+1-i}|$, and changing variable $t = -x$, we get

$$\begin{aligned}\delta_{i,j} &= \frac{1}{|s_i|}\int_{s_i}\varphi_j(x)\mathrm{d}x = \frac{1}{|s_i|}\int_{\eta_i}^{\gamma_i}\varphi_j(x)\mathrm{d}x = \frac{1}{|s_i|}\int_{-\eta_i}^{-\gamma_i} -\varphi_j(-t)\mathrm{d}t \\ &= \frac{1}{|s_{N_{\mathrm{loc}}+1-i}|}\int_{-\gamma_i}^{-\eta_i}\varphi_j(-t)\mathrm{d}t = \frac{1}{|s_{N_{\mathrm{loc}}+1-i}|}\int_{s_{N_{\mathrm{loc}}+1-i}}\varphi_j(-t)\mathrm{d}t.\end{aligned}$$

In the above computation, it is understood that, when $|s_i| = 0$ and hence s_i is a point ξ_i, the average on s_i means evaluation on ξ_i. By the uniqueness of the Lagrange functions, $\varphi_j(x) = \varphi_{N_{\mathrm{loc}}+1-j}(-x)$. □

Lemma 1 and Proposition 2 helps in localizing the zeros of the Lagrange functions associated with the histopolation problem (16). Nonetheless, they imply a weaker result compared to usual nodal Lagrange functions. In fact, the zeros of these latter polynomials are all contained in the set of nodes $\{\xi_i\}_{i=1}^{N_{\mathrm{loc}}}$ generating the interpolation

conditions. In contrast, the cardinality of the set containing the zeros of all the (either normalized or not) segmental Lagrange bases exceeds the dimension of the polynomial space. This difference can be explicitly observed comparing the panels of Figure 1. This fact affects the meaning of the location parameters that we select to relate such cardinal functions and the relative supports. Nevertheless, such polynomials still bear the following useful feature.

Lemma 2 *Let* $\{\varphi_i\}_{i=1}^{N_{\text{loc}}}$ *be the cardinal functions associated with disjoint supports* $\{s_i\}_{i=1}^{N_{\text{loc}}}$. *Then*

$$\sum_{i=1}^{N_{\text{loc}}} \varphi_i(x) = 1$$

for each $x \in I$.

Proof Expanding the solution of the histopolation problem (16) with respect to the Lagrange basis, one has

$$p(x) = \sum_{i=1}^{N_{\text{loc}}} \left(\frac{1}{|s_i|} \int_{s_i} f(x)\mathrm{d}x \right) \varphi_i(x),$$

see [23, Eq. (13)]. Since the histopolation operator is a projector [22, Section 4.4] onto degree $N_{\text{loc}} - 1$ polynomials, constants are reproduced. Hence, histopolating the function $f(x) = 1$, we obtain

$$1 = \sum_{i=1}^{N_{\text{loc}}} \left(\frac{1}{|s_i|} \int_{s_i} 1\mathrm{d}x \right) \varphi_i(x) = \sum_{i=1}^{N_{\text{loc}}} \varphi_i(x).$$

□

It is worth pointing out that a variant of Lemma 2 holds also for the Lagrange functions associated with the projector (15) (i.e., for discontinuous discretizations) if the segments s_i share the same length $|s_i| = |s|$ for each $i = 1, \ldots, N_{\text{loc}}$. By the last line of the proof of Lemma 2, in such a case we deduce

$$1 = \sum_{i=1}^{N_{\text{loc}}} |s_i| \varphi_i(x) = |s| \sum_{i=1}^{N_{\text{loc}}} \varphi_i(x),$$

whence $\sum_{i=1}^{N_{\text{loc}}} \varphi_i(x) = 1/|s|$. That this situation always corresponds to a unisolvent family has been shown in [21, Remark 3.4], and can be further deduced from the base case of [26, Proposition 3.14].

Remark 5 Lagrange bases for this kind of problems arise in edge elements [37], and explicit representation formulas are known in very few cases, generally obtained by imposing constraints on the supporting segments, see [22]. In all other cases, Proposition 1 is invoked.

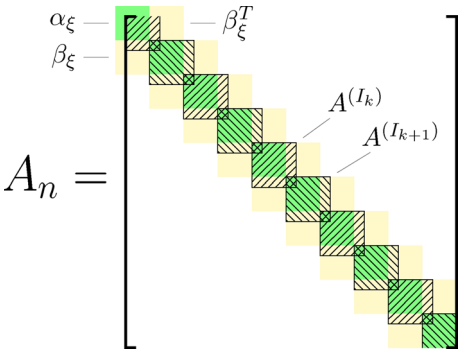

Fig. 2 Structure of the stiffness matrix and of the Toeplitz matrix. Element contributions are hatched in black: note the overlap of nearby blocks and the smaller first and last block. The blocks of the Toeplitx matrix are shaded in color (color figure online)

3 Spectral symbol and spectral theory

The present section is devoted to the spectral and structure analysis of the stiffness matrix (11) for fixed dimension and for the related sequences of matrices generated as the mesh size parameter tends to zero.

By a *sequence of matrices* we mean any sequence of the form $\{A_n\}_n$, where A_n is a square matrix of monotonically strictly increasing size d_n. Furthermore, for an integer $r \geq 1$, we use the term *r-block matrix-sequence* to indicate a special sequence of matrices of size $d_n = r\phi_n$, with $\{\phi_n\}_n$ being a strictly increasing sequence of positive integers. In the sequence formed by the stiffness matrices A_n given in (11), the parameter n represents the number of elements. To study such a sequence, we employ the concept of spectral distribution of a matrix-sequence, and in particular the properties of the $*$-algebra of block GLT sequences. The reader is referred to [33, 34] for a detailed exposition, while the results exploited in this paper are recalled in Appendix A.

To begin with, we explicitly provide a function that describes the spectrum of the sequence A_n in an asymptotic sense. This function is the *symbol*. To construct it, we follow the assembly procedure of the stiffness matrix, which is depicted in Figure 2.

From now on, we consider one-dimensional continuous elements. In this context, weights-based degrees of freedom are either evaluation at points, so we let $\{\xi_i\}_{i=1}^{r+1}$ be a set of reference positions in $\widehat{I} = [0, 1]$, or the averaging functionals discussed in Section 2.2. The presence of both extrema of the interval is needed for defining continuous elements, thus we assume that $\xi_1 = 0$ and $\xi_{r+1} = 1$ for the former case. For the latter, we thus assume that the extremal supports s_1 and s_{r+1} shrink to nodes $\xi_1 = 0$ and $\xi_{r+1} = 1$.

Let then $A^{(I_k)}$ be the $(r+1) \times (r+1)$ local contribution of element I_k to the global stiffness matrix, defined as in (12). In the simple case of a unit diffusion coefficient ($b(x) = 1$) and uniform mesh size, then $A^{(I_k)} = A^{\text{loc}}$ is independent of k and the stiffness matrix has the structure of a block-tridiagonal Toeplitz matrix with $r \times r$ blocks (see Figure 2). We are thus able to write the spectral symbol $f_r^{\xi} : [-\pi, \pi] \to \mathbb{C}^{r \times r}$ of the stiffness matrix as a function depending on the ξ_i's.

Let us consider a uniform grid with n elements and let A_n be the corresponding stiffness matrix (11). Consider the set of global indices $\mathcal{I}_m \doteq \{\text{LTG}(i, m) : i =$

$0, \dots, r\}$ associated with a generic m-th element (with $m \neq 1, n$ since the first and last elements are influenced by the boundary conditions). Since the contribution of the shape function associated with $\xi_{r+1} = 1$ of each element overlaps in A_n with those of the shape function associated with $\xi_1 = 0$ of the next element, the submatrix of A_n for the rows and columns in $\mathcal{I}_m$ is

$$(A_\xi)_{i,j} \doteq \begin{cases} A^{\text{loc}}_{1,1} + A^{\text{loc}}_{r+1,r+1} & \text{if } (i,j) = (1,1) \text{ or } (r+1, r+1), \\ A^{\text{loc}}_{i,j} & \text{otherwise.} \end{cases}$$

The structure of the $(r+1) \times (r+1)$ matrix A_ξ is

$$A_\xi = \left[\begin{array}{c|c} \alpha_\xi & \widetilde{\beta}_\xi^T \\ \hline \widetilde{\beta}_\xi & b \end{array}\right], \tag{17}$$

where $\alpha_\xi \in \mathbb{R}^{r\times r}$, $\widetilde{\beta}_\xi \in \mathbb{R}^{1\times r}$, $b \in \mathbb{R}$ and $b = (\alpha_\xi)_{1,1}$. Following [52], define

$$\beta_\xi \doteq \left[\begin{array}{c} \widetilde{\beta}_\xi \\ \hline \mathbf{0} \end{array}\right],$$

with $\mathbf{0}$ being the zero matrix of size $(r-1) \times r$, so that $\beta_\xi \in \mathbb{R}^{r\times r}$.

Taking into consideration the notion of generating function for Toeplitz structures reported in A.2, we observe that the stiffness matrix A_n is a principal submatrix of size $nr - 1$ of the Toeplitz matrix $T_n(f_r^\xi)$ with generating function

$$\begin{aligned} f_r^\xi : \quad & [-\pi, \pi] \to \mathbb{C}^{r\times r}, \\ & \theta \mapsto \alpha_\xi + \beta_\xi e^{i\theta} + \beta_\xi^T e^{-i\theta}. \end{aligned} \tag{18}$$

Furthermore, with reference to [14, Chapter 5, pp. 85-86], according to the first item of axiom **GLT3** and to axiom **GLT1**, we deduce that f_r^ξ is also the spectral and the singular value symbol of $\{T_n(f_r^\xi)\}_n$, in the sense of Definition 2 with $t = 2$. As a first conclusion we infer that f_r^ξ is the spectral and the singular value symbol of the stiffness matrix-sequence $\{A_n\}_n$. This is proven by applying Theorem 3 to $X_n = T_n(f_r^\xi)$, $A_n = P_n^* X_n P_n$, $d_n = nr$, $\delta_n = nr - 1$, so that $\delta_n/d_n \to 1$ as $n \to \infty$, and P_n rectangular matrix obtained by the identity of size d_n by eliminating only the last column.

As a consequence, the union of the ranges of the r eigenvalues $\lambda_1(f_r^\xi) \le \lambda_2(f_r^\xi) \le \cdots \le \lambda_r(f_r^\xi)$ is a weak cluster of the eigenvalues of both $\{T_n(f_r^\xi)\}_n$ and $\{A_n\}_n$, in accordance with Definition 3 and the subsequent Remark 15.

3.1 Determinant of the symbol

The aim of this section is to provide an explicit formula for the determinant of the symbol (18). Recall that, in the case of the equidistributed Lagrangian elements (i.e.

$\xi_i = (i-1)/r$ for $i = 1, \ldots, r+1$), one has

$$\det f_r(\theta) = d_r(2 - 2\cos(\theta)),$$

where

$$d_r \doteq \det\left[\langle \ell_i', \ell_j' \rangle\right]_{i,j=2}^{r} \tag{19}$$

and $\{\ell_i\}_{i=1}^{r+1}$ is the Lagrangian basis associated with *equispaced* nodes in $[0, 1]$. For the proof, see [35, Theorem 8], two ingredients are employed. The first is basic and concerns the properties of the determinant, when expanding its computation along rows and columns. The second ingredient is the relation

$$\det(f_r(0)) = d_r + 2d_r' + d_r'' = 0 \quad \text{and} \quad d_r + d_r' = 0,$$

with d_r' and d_r'' defined as in [35, Eq. (45)], which can be easily proven once the equality

$$\sum_{j=1}^{r+1} \ell_i'(x) = 0$$

is established. In order to extend the result on $\det f_r$ to the case of bases induced by weights and hence to $\det f_r^{\xi}$, we need to generalize the previous result.

Lemma 3 *Let $\{\varphi_i\}_{i=1}^{r+1}$ the basis for $\mathbb{P}_r$ induced by weights corresponding to evaluations on $\{\xi_i\}_{i=1}^{r+1}$. Then*

$$\sum_{i=1}^{r+1} \varphi_i'(x) = 0.$$

Moreover, any choice of r polynomials out of $\{\varphi_i'\}_{i=1}^{r+1}$ is a basis for $\mathbb{P}_{r-1}$.

Proof We start by defining $q(x)$ as the degree r polynomial

$$q(x) \doteq \sum_{i=1}^{r+1} \varphi_i(x) - 1.$$

As the basis $\{\varphi_i\}_{i=1}^{r+1}$ is dual to weights associated with $\{\xi_i\}_{i=1}^{r+1}$, one has $q(\xi_i) = 0$ for each ξ_i, whence $q(x) = 0$ and so $\sum_{i=1}^{r+1} \varphi_i(x) = 1$ identically. By differentiating both sides one obtains the first claim. The second part of the proof is identical to that already known for the Lagrange basis (see [35]). □

Equation (14) motivates the following computation.

Proposition 3 *Let $V_{i,j} = \ell_j(\xi_i)$ be the Vandermonde matrix written with respect to the uniform Lagrangian basis $\{\ell_i\}_{i=1}^{r+1}$ and some general collection of points $\{\xi_i\}_{i=1}^{r+1}$*

such that $\xi_1 = 0$ *and* $\xi_{r+1} = 1$. *Then*

$$V^{-1} = \left[\begin{array}{c|c|c} 1 & \mathbf{0} & 0 \\ \hline -\boldsymbol{x}_V & (V')^{-1} & -\boldsymbol{y}_V \\ \hline 0 & \mathbf{0} & 1 \end{array}\right], \tag{20}$$

where $V' \doteq [V_{i,j}]_{i,j=2}^{r}$ *and* $\boldsymbol{x}_V \doteq (V')^{-1}\boldsymbol{x}$ *and* $\boldsymbol{y}_V \doteq (V')^{-1}\boldsymbol{y}$, *with* $\boldsymbol{x} = [V_{i,1}]_{i=2}^{r}$ *and* $\boldsymbol{y} = [V_{i,r+1}]_{i=2}^{r}$.

Proof Since $\xi_1 = 0$ and $\xi_{r+1} = 1$, $V_{1,j} = \ell_j(\xi_1) = \delta_{j,1}$ and $V_{r+1,j} = \ell_j(\xi_{r+1}) = \delta_{j,r+1}$. Thus

$$V = \left[\begin{array}{c|c|c} 1 & \mathbf{0} & 0 \\ \hline \boldsymbol{x} & V' & \boldsymbol{y} \\ \hline 0 & \mathbf{0} & 1 \end{array}\right] = \left[\begin{array}{c|c|c} 1 & \mathbf{0} & 0 \\ \hline \mathbf{0} & V' & \mathbf{0} \\ \hline 0 & \mathbf{0} & 1 \end{array}\right] + \begin{bmatrix} 0 \\ \boldsymbol{x} \\ 0 \end{bmatrix} \boldsymbol{e}_1^T + \begin{bmatrix} 0 \\ \boldsymbol{y} \\ 0 \end{bmatrix} \boldsymbol{e}_{r+1}^T = \left[\begin{array}{c|c|c} 1 & \mathbf{0} & 0 \\ \hline \mathbf{0} & V' & \mathbf{0} \\ \hline 0 & \mathbf{0} & 1 \end{array}\right] + \begin{bmatrix} 0 & 0 \\ \boldsymbol{x} & \boldsymbol{y} \\ 0 & 0 \end{bmatrix} \left[\begin{array}{c} \boldsymbol{e}_1^T \\ \hline \boldsymbol{e}_{r+1}^T \end{array}\right].$$

Let us denote $U_V \doteq \begin{bmatrix} 0 & 0 \\ \boldsymbol{x}_V & \boldsymbol{y}_V \\ 0 & 0 \end{bmatrix}$. We compute

$$\begin{aligned} V^{-1} &= \left(\left[\begin{array}{c|c|c} 1 & \mathbf{0} & 0 \\ \hline \mathbf{0} & V' & \mathbf{0} \\ \hline 0 & \mathbf{0} & 1 \end{array}\right] \left(I + U_V \left[\begin{array}{c} \boldsymbol{e}_1^T \\ \hline \boldsymbol{e}_{r+1}^T \end{array}\right] \right) \right)^{-1} \\ &= \left(I + U_V \left[\begin{array}{c} \boldsymbol{e}_1^T \\ \hline \boldsymbol{e}_{r+1}^T \end{array}\right] \right)^{-1} \left[\begin{array}{c|c|c} 1 & \mathbf{0} & 0 \\ \hline \mathbf{0} & (V')^{-1} & \mathbf{0} \\ \hline 0 & \mathbf{0} & 1 \end{array}\right] \\ &= \left[I - U_V \left(I_2 + \left[\begin{array}{c} \boldsymbol{e}_1^T \\ \hline \boldsymbol{e}_{r+1}^T \end{array}\right] U_V \right)^{-1} \left[\begin{array}{c} \boldsymbol{e}_1^T \\ \hline \boldsymbol{e}_{r+1}^T \end{array}\right] \right] \left[\begin{array}{c|c|c} 1 & \mathbf{0} & 0 \\ \hline \mathbf{0} & (V')^{-1} & \mathbf{0} \\ \hline 0 & \mathbf{0} & 1 \end{array}\right] \\ &= \left[I - U_V \left[\begin{array}{c} \boldsymbol{e}_1^T \\ \hline \boldsymbol{e}_{r+1}^T \end{array}\right] \right] \left[\begin{array}{c|c|c} 1 & \mathbf{0} & 0 \\ \hline \mathbf{0} & (V')^{-1} & \mathbf{0} \\ \hline 0 & \mathbf{0} & 1 \end{array}\right] \\ &= \left[\begin{array}{c|c|c} 1 & \mathbf{0} & 0 \\ \hline \mathbf{0} & (V')^{-1} & \mathbf{0} \\ \hline 0 & \mathbf{0} & 1 \end{array}\right] - U_V \left[\begin{array}{c} \boldsymbol{e}_1^T \\ \hline \boldsymbol{e}_{r+1}^T \end{array}\right] = \left[\begin{array}{c|c|c} 1 & \mathbf{0} & 0 \\ \hline -\boldsymbol{x}_V & (V')^{-1} & -\boldsymbol{y}_V \\ \hline 0 & \mathbf{0} & 1 \end{array}\right], \end{aligned}$$

where the above identities are granted by the Sherman-Morrison-Woodbury formula (see [39, p. 65] and related references therein). □

The following result is then a straightforward consequence of Laplace's Theorem applied twice to V.

Lemma 4 *Under the same hypotheses of Proposition 3, one has*

$$\det V = \det V'.$$

Lemma 4 shows that the determinant of the above $(r+1)\times(r+1)$ matrix can be in fact computed by considering a $(r-1)\times(r-1)$ minor, and it is the key fact for proving the following result.

Theorem 1 *Let $f_r^{\xi}(\theta)$ be the symbol (18) associated with the Laplacian operator discretized with weights induced by points $\{\xi_i\}_{i=1}^{r+1}$, with $\xi_1 = 0$ and $\xi_{r+1} = 1$. Then*

$$\det f_r^{\xi}(\theta) = \left(\det(V^{-1})\right)^2 d_r(2-2\cos(\theta)), \tag{21}$$

where d_r is defined in (19).

Proof Consider A^{loc} and B^{loc} and recall that they are related as in Proposition 1, Eq. (14). We put

$$A' \doteq [A^{\mathrm{loc}}_{i,j}]_{i,j=2}^{r+1},\ A'' \doteq [A^{\mathrm{loc}}_{i,j}]_{i,j=2}^{r} \quad \text{and} \quad B' \doteq [B^{\mathrm{loc}}_{i,j}]_{i,j=2}^{r+1},\ B'' \doteq [B^{\mathrm{loc}}_{i,j}]_{i,j=2}^{r}.$$

From [35, Lemma 9], we know that

$$\det B' = \det\left[\langle \ell_i', \ell_j'\rangle\right]_{i,j=2}^{r+1} = \det\left[\langle \ell_i', \ell_j'\rangle\right]_{i,j=2}^{r} = d_r = \det B''.$$

Let us denote

$$d_r^{\xi} \doteq \det A'' = \det\left[\langle \varphi_i', \varphi_j'\rangle\right]_{i,j=2}^{r}.$$

Following (14) and (20), we compute

$$\begin{aligned}
A^{\mathrm{loc}} &= V^{-T} B^{\mathrm{loc}} V^{-1} \\
&= \left[\begin{array}{c|c|c} 1 & -\boldsymbol{x}_V^T & 0 \\ \hline \mathbf{0} & (V')^{-T} & \mathbf{0} \\ \hline 0 & -\boldsymbol{y}_V^T & 1 \end{array}\right] \left[\begin{array}{c|c|c} * & * & * \\ \hline * & B'' & * \\ \hline * & * & * \end{array}\right] \left[\begin{array}{c|c|c} 1 & \mathbf{0} & 0 \\ \hline -\boldsymbol{x}_V & (V')^{-1} & -\boldsymbol{y}_V \\ \hline 0 & \mathbf{0} & 1 \end{array}\right] \\
&= \left[\begin{array}{c|c|c} * & * & * \\ \hline \mathbf{0} & (V')^{-T} B'' & \mathbf{0} \\ \hline * & * & * \end{array}\right] \left[\begin{array}{c|c|c} 1 & \mathbf{0} & 0 \\ \hline -\boldsymbol{x}_V & (V')^{-1} & -\boldsymbol{y}_V \\ \hline 0 & \mathbf{0} & 1 \end{array}\right] \\
&= \left[\begin{array}{c|c|c} * & * & * \\ \hline * & (V')^{-T} B'' (V')^{-1} & * \\ \hline * & * & * \end{array}\right].
\end{aligned}$$

As a consequence $A'' = (V')^{-T} B'' (V')^{-1}$, whence $d_r^{\xi} = \left(\det(V')^{-1}\right)^2 d_r$ and Lemma 4 thus immediately yields $d_r^{\xi} = \left(\det(V^{-1})\right)^2 d_r$. To obtain the claim of Eq. (21), it is now sufficient to retrace the proof of [35, Theorem 8], whose applicability is granted by Lemma 3. □

Remark 6 Exploiting Lemma 2, one immediately obtains that all the results proved in this section apply also to elements generated by Lagrange bases for (normalized) histopolation. In applications related with such a case, it is not convenient to interpret

the parameter ξ as representing the set of unknown nodes that realize the mean value theorem, due to Proposition 2. We propose a meaning for such a quantity in the subsequent Section 4. Likewise, the Vandermonde matrix appearing in Eq. (21) is thus replaced by the *generalized* Vandermonde matrix discussed in [23, Section 4].

3.2 Extremal eigenvalues and conditioning

A remarkable feature pointed out in the analysis of equidistributed Lagrangian elements applied to the Laplacian is that eigenvalues functions of the spectral symbol are well separated [52]; hence, there is only one of them having a zero at $\theta = 0$. We exploit formula (21) to extend such a result to our framework.

Proposition 4 *The south-east principal minor S_ξ of $f_r^\xi(\theta)$ of size $(r-1)\times(r-1)$ has all the entries independent of θ and* $\det S_\xi \neq 0$. *In particular, the minimal eigenvalue m of S_ξ is strictly positive.*

Proof Let us define the south-east minor

$$S_\xi \doteq \left[f_r^\xi\right]_{i,j=2}^{r} \in \mathbb{R}^{(r-1)\times(r-1)}.$$

By direct inspection of relation (18) we see that all its entries are independent of θ, see also Figure 2. Since $f_r^\xi(\theta)$ is positive semidefinite, the matrix S_ξ has to be also positive semidefinite so that its determinant is nonnegative. We claim that $\det S_\xi > 0$. In fact, let us suppose by contradiction that $\det(S_\xi) = 0$. Then there exists an eigenvalue $\lambda_1 = 0$. The minor S_ξ is independent of θ, hence the eigenvalues interlacing theorem implies that the eigenvalue function $\lambda_1(f_r^\xi(\theta))$ is identically zero and the latter is in contrast with (21). Hence $m = \lambda_1(S_\xi) > 0$. □

The previous result is quite important since in turn it allows to deduce directly the following theorem, which generalizes [52, Theorem 4] to the framework of weights for continuous elements.

Theorem 2 *For the symbol $f_r^\xi(\theta)$, the following statements hold:*

1. *there exist constants $C_1, C_2 > 0$ (dependent on f_r^ξ) such that*

$$C_1 \sum_{j=1}^{r}(2-2\cos(\theta_j)) \leq \lambda_1(f_r^\xi(\theta)) \leq C_2 \sum_{j=1}^{r}(2-2\cos(\theta_j)); \tag{22}$$

2. *there exist constants $m, M > 0$ (dependent on f_r^ξ) such that*

$$0 < m \leq \lambda_j(f_r^\xi(\theta)) \leq M, \quad j = 2,\dots,r. \tag{23}$$

Further, $m = \lambda_1(S_\xi) > 0$ is the quantity appearing in the last line of the proof of Proposition 4.

Proof Given the Hermitian character of $f_r^{\xi}(\theta)$ for every θ, the two statements directly follow from the use of the interlacing theorem and from Proposition 4, taking into account Theorem 1. □

Remark 7 A practical consequence of (23) is that graphs of the eigenvalue functions $\lambda_i(f_r^{\xi}(\theta))$ are separated in a weak sense. For the case of equidistributed Lagrangian, this separation is in particular strong [52]. In the case of weights, this separation may be weak depending on the value of ξ (see Figure 4).

For any choice of $\{\xi_i\}_{i=1}^{r+1}$ such that the generalized Vandermonde matrix is invertible, the sequence of stiffness matrices is distributed as the symbol f_r^{ξ}. Thus the union of the ranges of the eigenvalue functions of f_r^{ξ} represent a cluster for their spectra, while their convex hull contains all the eigenvalues of the involved matrices.

Remark 8 From Theorem 2, we know that the minimal eigenvalue function of f_r^{ξ} behaves as the symbol of the standard finite difference Laplacian, while the other eigenvalue functions are well separated from zero and bounded. Furthermore, thanks to the analysis in [57], the fact that the minimal eigenvalue of f_r^{ξ} has a zero of order two implies that

- the minimal eigenvalue goes to zero as n^{-2},
- the maximal eigenvalue converges from below to the maximum of the maximal eigenvalue function of f_r^{ξ},

and hence

- the conditioning of A_n grows asymptotically as n^2.

The constants of proportionality are studied in Section 4 and given more precisely in Eq. (27).

We conclude this section with an analysis of the kernel of f_r^{ξ}. It follows from Proposition 4 that there is only an eigenvalue of f_r^{ξ} that assumes the value 0 for $\theta = 0$. As a consequence, $\ker\{f_r^{\xi}(0)\}$ is generated by one vector. The following proposition shows that such a vector is independent of $\{\xi_i\}_{i=1}^{r+1}$.

Proposition 5 *Let* $\mathbf{j} \doteq (j, \ldots, j)^T \in \mathbb{C}^r$. *For each* ξ *and* r, *one has*

$$f_r^{\xi}(0)\mathbf{1} = \mathbf{0}.$$

Proof By substituting $\theta = 0$ in (18), one immediately obtains that

$$f_r^{\xi}(0)\mathbf{1} = \left(\alpha_{\xi} + \beta_{\xi} + \beta_{\xi}^T\right)\mathbf{1}.$$

Since multiplying by $\mathbf{1}$ equals to taking sum row-wise, we are left to prove that

$$\sum_{i=1}^{r}\left(\alpha_{\xi} + \beta_{\xi} + \beta_{\xi}^T\right)_{j,i} = 0, \quad j = 1, \ldots, r.$$

Consider the splitting in Eq. (17). Plugging the definition of α_ξ and β_ξ in, for $j = 2, \dots, r$ one has

$$\sum_{i=1}^{r} \left(\alpha_\xi + \beta_\xi + \beta_\xi^T\right)_{j,i} = \sum_{i=1}^{r} \left\langle \varphi_j', \varphi_i' \right\rangle + \left\langle \varphi_j', \varphi_{r+1}' \right\rangle = \left\langle \varphi_j', \sum_{i=1}^{r+1} \varphi_i' \right\rangle = \left\langle \varphi_j', 0 \right\rangle = 0.$$

The equality $\sum_{i=1}^{r+1} \varphi_i' = 0$ is proved in Lemma 3. Similarly, for $j = 1$ one has

$$\begin{aligned}
&\sum_{i=1}^{r} \left(\alpha_\xi + \beta_\xi + \beta_\xi^T\right)_{1,i} \\
&\quad = \langle \varphi_1', \varphi_1' \rangle + \langle \varphi_{r+1}', \varphi_{r+1}' \rangle + \sum_{i=2}^{r} \langle \varphi_1', \varphi_i' \rangle + \langle \varphi_1', \varphi_{r+1}' \rangle + \sum_{i=1}^{r} \langle \varphi_{r+1}', \varphi_i' \rangle \\
&\quad = \sum_{i=1}^{r+1} \langle \varphi_1', \varphi_i' \rangle + \sum_{i=1}^{r+1} \langle \varphi_{r+1}', \varphi_i' \rangle = \left\langle \varphi_1', \sum_{i=1}^{r+1} \varphi_i' \right\rangle + \left\langle \varphi_{r+1}', \sum_{i=1}^{r+1} \varphi_i' \right\rangle = 0.
\end{aligned}$$

The claim is proved. □

Remark 9 Since $\dim \ker\{f_r^\xi(0)\} = 1$, as an immediate corollary we obtain that $\ker\{f_r^\xi(0)\} = \langle \mathbf{1} \rangle$. We notice that the latter property is exactly the same in the case of the spectral symbol occurring with standard finite element approximations as in [52, Theorem 4, item 1].

Remark 10 In contrast with Section 3.1, Lemma 2 by itself is not sufficient to extend results of the present section to the symbol of stiffness matrices associated with the finite elements arising from normalized histopolation discussed in Section 2.2. In fact, to retrieve the correct counterpart of Proposition 5, one must also require the continuity of the finite element space, shrinking supports s_1 and s_{r+1} to the endpoints of the reference interval I, to avoid the filling of the matrix β_ξ. The same ansatz then gives also the other results of the section.

4 Optimization of weights

We apply the spectral theory of Section 3 to the case of weights introduced in Section 2.1 and Section 2.2. We analyze in depth the case of continuous univariate functions, as up to degree $r = 4$ the whole problem can be handled by introducing only one location parameter. Nevertheless, the theory so far illustrated does not impose any structural changes as a consequence of larger dimensions, provided that Lemma 3 is consistently replaced. The multivariate case, which forces the introduction of several location parameters, will be treated in companion papers.

4.1 Constant coefficients

Let us first suppose that $b(x) = 1$ and that the mesh is uniform. We now exploit the results of Section 3 (see also the machinery recalled in Appendix A) to explicitly optimize the placement of weights in the cases $r = 3$ and $r = 4$.

Nodal degrees of freedom. When $r = 3$, a basis for weights is dual to four evaluations on $\{\xi_i\}_{i=1}^4$ in the reference element $\widehat{I} = [0, 1]$; this makes degree 3 the first nontrivial case. Since global continuity requires $\xi_1 = 0$ and $\xi_4 = 1$, we are left with the placement of ξ_2 and ξ_3. Adding the hypothesis of symmetry, one immediately gets that $\xi_3 = 1-\xi_2$. We thus drop indices and consider only one parameter ξ, so that nodes in $\widehat{I}$ are $\{0, \xi, 1-\xi, 1\}$.

Since $b(x) = 1$ and the mesh is uniform, the local contribution of each element is constant and, recalling Eq. (12), we obtain that

$$A^{\text{loc}} = \begin{pmatrix} \frac{15\xi^4-30\xi^3+15\xi^2+2}{15\xi^2(1-\xi)^2} & \frac{4-5\xi}{30\xi^2(1-\xi)^2(2\xi-1)} & \frac{1-5\xi}{30\xi^2(1-\xi)^2(2\xi-1)} & \frac{-30\xi^4+60\xi^3-30\xi^2+1}{30\xi^2(1-\xi)^2} \\ \frac{4-5\xi}{30\xi^2(1-\xi)^2(2\xi-1)} & \frac{5\xi^2-5\xi+2}{15\xi^2(1-\xi)^2(2\xi-1)^2} & \frac{10\xi^2-10\xi+1}{30\xi^2(2\xi-1)^2(1-\xi)^2} & \frac{1-5\xi}{30\xi^2(1-\xi)^2(2\xi-1)} \\ \frac{1-5\xi}{30\xi^2(1-\xi)^2(2\xi-1)} & \frac{10\xi^2-10\xi+1}{30\xi^2(2\xi-1)^2(1-\xi)^2} & \frac{5\xi^2-5\xi+2}{15\xi^2(2\xi-1)^2(\xi-1)^2} & \frac{4-5\xi}{30\xi^2(1-\xi)^2(2\xi-1)} \\ \frac{-30\xi^4+60\xi^3-30\xi^2+1}{30\xi^2(1-\xi)^2} & \frac{1-5\xi}{30\xi^2(1-\xi)^2(2\xi-1)} & \frac{4-5\xi}{30\xi^2(1-\xi)^2(2\xi-1)} & \frac{15\xi^4-30\xi^3+15\xi^2+2}{15\xi^2(1-\xi)^2} \end{pmatrix}.$$

Following the construction at the beginning of Section 3, the spectral symbol is the function

$$\begin{aligned} f_3^\xi : \quad [-\pi, \pi] &\to \mathbb{C}^{3\times 3}, \\ \theta &\mapsto \alpha_\xi + \beta_\xi e^{i\theta} + \beta_\xi^T e^{-i\theta}, \end{aligned} \tag{24}$$

being

$$\alpha_\xi = \begin{pmatrix} \frac{30\xi^4-60\xi^3+30\xi^2+4}{15\xi^2(1-\xi)^2} & \frac{4-5\xi}{30\xi^2(1-\xi)^2(2\xi-1)} & \frac{1-5\xi}{30\xi^2(1-\xi)^2(2\xi-1)} \\ \frac{4-5\xi}{30\xi^2(1-\xi)^2(2\xi-1)} & \frac{5\xi^2-5\xi+2}{15\xi^2(1-\xi)^2(2\xi-1)^2} & \frac{10\xi^2-10\xi+1}{30\xi^2(2\xi-1)^2(1-\xi)^2} \\ \frac{1-5\xi}{30\xi^2(1-\xi)^2(2\xi-1)} & \frac{10\xi^2-10\xi+1}{30\xi^2(2\xi-1)^2(1-\xi)^2} & \frac{5\xi^2-5\xi+2}{15\xi^2(2\xi-1)^2(\xi-1)^2} \end{pmatrix}$$

and

$$\beta_\xi = \begin{pmatrix} \frac{-30\xi^4+60\xi^3-30\xi^2+1}{30\xi^2(1-\xi)^2} & \frac{1-5\xi}{30\xi^2(1-\xi)^2(2\xi-1)} & \frac{4-5\xi}{30\xi^2(1-\xi)^2(2\xi-1)} \\ 0 & 0 & 0 \\ 0 & 0 & 0 \end{pmatrix}.$$

Direct computation shows that

$$\det(f_\xi(\theta)) = \frac{-e^{-i\theta}\left(1 + e^{2i\theta} - 2e^{i\theta}\right)}{60\xi^4(2\xi-1)^2(\xi-1)^4} = \frac{2 - 2\cos(\theta)}{60\xi^4(2\xi-1)^2(\xi-1)^4}, \tag{25}$$

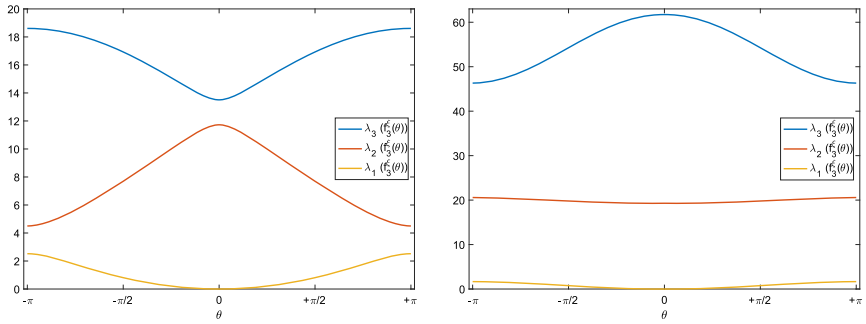

Fig. 3 Eigenvalues functions of $f_3^\xi(\theta)$ for $\xi = 0.28$ (left) and $\xi = 0.10$ (right)

which is defined when $\xi \neq 0, \frac{1}{2}, 1$ (i.e. under the natural assumption that the nodes are pairwise distinct). Let us denote by $\lambda_j(f_3^\xi(\theta))$, $j = 1, 2, 3$, the eigenvalues of $f_3^\xi(\theta)$ ordered nondecreasingly. Theorem 2 shows that

$$\lambda_1(f_3^\xi(0)) = 0. \tag{26}$$

Moreover, Remark 7 ensures that the graphs of the the eigenvalues $\lambda_j(f_3^\xi(\theta))$, $j = 1, 2, 3$, do not intersect for each ξ. This is depicted in Figure 3 for $r = 3$ and in Figure 4 for $r = 4$; in both cases two distinct values of ξ are offered. This latter image also shows that the separation is weak: in the right hand side panel, the minimum of the second eigenvalue is approaching the maximum of the smallest one. Finally notice that, in contrast with the minimum of the smallest eigenvalue, which is exactly zero due to Theorem 2, features of the maximum of the largest eigenvalue depend on the value of ξ. This can be again appreciated by comparing the panels of both Figure 3 and Figure 4.

The trend of $\lambda_1(f_3^\xi(\theta))$ as $\theta \to 0$ is prescribed by the order of the operator and does *not* depend on ξ (see Figure 3, red line). Expanding (25) about $\theta = 0$, we obtain

$$\begin{aligned}\lambda_1(f_3^\xi(\theta)) &= \frac{\det(f_3^\xi(\theta))}{\lambda_2(f_3^\xi(\theta))\lambda_3(f_3^\xi(\theta))} \\ &= \theta^2 \frac{4\xi^4 - 12\xi^3 + 13\xi^2 - 6\xi + 1}{3(2\xi - 1)^2(\xi - 1)^2} + O(\theta^4) = \frac{\theta^2}{3} + O(\theta^4).\end{aligned}$$

We aim at containing the conditioning κ_2 of the stiffness matrix A_n, which is equal to the function

$$\kappa_2(n, \xi) = \frac{\lambda_{\max}(A_n)}{\lambda_{\min}(A_n)}.$$

From Remark 8 and the fact that $\lambda_1(f_3^\xi(\theta))$ has a zero of order two at $\theta = 0$ and $\max_\theta \lambda_3(f_3^\xi(\theta)) - \lambda_3(f_3^\xi(\theta))$ has also a zero of order two for $\theta = \arg\max_\zeta \lambda_3(f_3^\xi(\zeta))$,

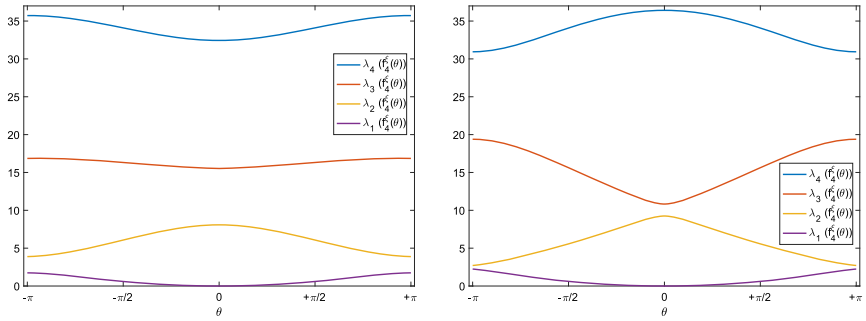

Fig. 4 Eigenvalues functions of $f_4^{\xi}(\theta)$ for $\xi = 0.12$ (left) and $\xi = 0.22$ (right)

using the results in [57], we have

$$\kappa_2(n,\xi) = n^2 \frac{\max_\theta \lambda_3(f_3^{\xi}(\theta)) - c_1 n^{-2} + O(n^{-3})}{c_2\left(1 + O(n^{-2})\right)} = \frac{n^2 \max_\theta \lambda_3(f_3^{\xi}(\theta))}{c_2}\left(1 + O(n^{-2})\right), \tag{27}$$

with

$$c_1 = -\lambda_3''(f_3^{\xi}(0))/2 > 0 \quad \text{and} \quad c_2 = \lambda_1''(f_3^{\xi}(0))/2 > 0.$$

We thus look for values of ξ that minimize $\sup_\xi \lambda_3$. In contrast with $\lambda_1(f_r^{\xi}(\theta))$, the maximum of $\lambda_3(f_r^{\xi}(\theta))$ is not necessarily attained at 0. In particular, this depends on the value of ξ (see Figure 3; Figure 4 also shows that the same happens for the case $r = 4$).

As a consequence, explicit expressions for $\lambda_3(f_r^{\xi}(\theta))$ or even for $\sup_\xi \lambda_3(f_r^{\xi}(\theta))$ are not easily derivable. Thus, in order to optimize the conditioning, we perform a sampling of $\xi \in (0, \frac{1}{2})$ and compute the quantity (27).

The left panel of Figure 5 reports the quantity $\kappa_2(n,\xi)$ as ξ varies. As evident from the graph, around the minimum of the curves there is a fairly large interval positions of the internal nodes in which any choice of ξ reduces the conditioning of the spectral symbol (the blue line) and hence of the whole stiffness matrix. This can be exploited in applications by choosing convenient values for ξ. Inspecting the results, one finds that the minimum conditioning is attained at $\xi \approx 0.29$ for $r = 3$.

Remark 11 When $\xi \to 0$ and $\xi \to 0.5$ some nodes coalesce, making the system ill-conditioned. The behavior of the conditioning close to such values of ξ is however different. In fact, when $\xi = 0$, the rank of the Vandermonde matrix V decreases by 2. When $\xi = 0.5$, it may decrease by 1 (for $r = 3$) or by 3 (for $r = 4$). This effect is visible in the asymmetry in $\kappa_2(n,\xi)$ in Figure 5.

Remark 12 Note that, as a first attempt, one may try to optimize the conditioning of A_n by minimizing the determinant of $f_3^{\xi}(\theta)$. For $r = 3$, this gives the value $\xi = \frac{1}{2} - \frac{1}{2\sqrt{5}} \approx$

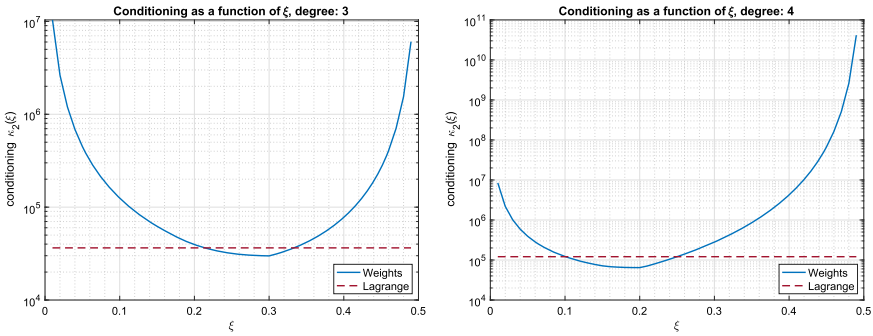

Fig. 5 A plot of the conditioning $\kappa_2(n, \xi)$ as ξ varies, in logarithmic scale. Here the diameter of the interval is $h = 1/64$ so that the matrix size n is fixed and the horizontal dashed red line represents the conditioning with respect to uniform nodes, namely those in duality with equidistributed Lagrangian elements. The cases $r = 3$ (left) and $r = 4$ (right) are depicted (color figure online)

0.28, thus leading to Gauss-Lobatto nodes. This is a consequence of Theorem 1. In fact, Gauss-Lobatto nodes maximizing the determinant of the Vandermonde matrix on an interval coincide with Fekete points [32]. We note that the value $\xi \approx 0.29$ is indeed close to Gauss-Lobatto nodes. For a weights-oriented study of Fekete problems we address to [23].

Remark 13 A similar analysis can be produced for any degree r. For $r = 4$ the problem can be handled again with only one parameter ξ, noticing that symmetric points obey $\left[0, \xi, \frac{1}{2}, 1-\xi, 1\right]$. Again, the eigenvalue functions $\lambda_j(f_4^{\xi}(\theta))$, $j = 1, 2, 3, 4$, are distinct and well separated, as shown in Figure 4. An analysis on the optimization of the determinant yields again Gauss-Lobatto points $\xi = \frac{1}{2} - \frac{\sqrt{3}}{2\sqrt{7}} \approx 0.17$ (see Remark 12 for an explanation), whereas a direct inspection of the graph in the right panel of Figure 5 shows that the optimal value is $\xi \approx 0.21$.

Segmental degrees of freedom. For the segmental degrees of freedom, corresponding to $k = 1$ and yielding the histopolation-based Lagrange bases introduced in Section 2.2, the situation becomes more involved. In the normalized case, which we need to enforce interelement continuity, explicit expressions for cardinal bases are not available. Hence they must be computed via Proposition 1.

For a degree r finite element method, we shall select $r + 1$ segments $\{s_i\}_{i=1}^{r+1}$ supported in the reference element $\widehat{I}$. To satisfy the hypothesis of interelement continuity we have to shrink the first and the last segments to the endpoints of the interval. As a consequence, $s_1 = 0$ and $s_{r+1} = 1$.

Each generic segment s_i is described by two parameters, yielding to an undetermined system, unless some constraints are imposed. We think of such parameters as the endpoints of segments, and restrict our study to supports that are pairwise symmetric with respect to the center of $\widehat{I}$.

For $r = 2$, we hence have $s_1 = [1/2 - \xi, 1/2 + \xi]$. Due to Proposition 2, this case is very close to the nodal case where $\xi_1 = 1/2$. We then turn to the cases $r = 3$ and $r = 4$. We may enforce symmetry, and exploit concatenation of segments,

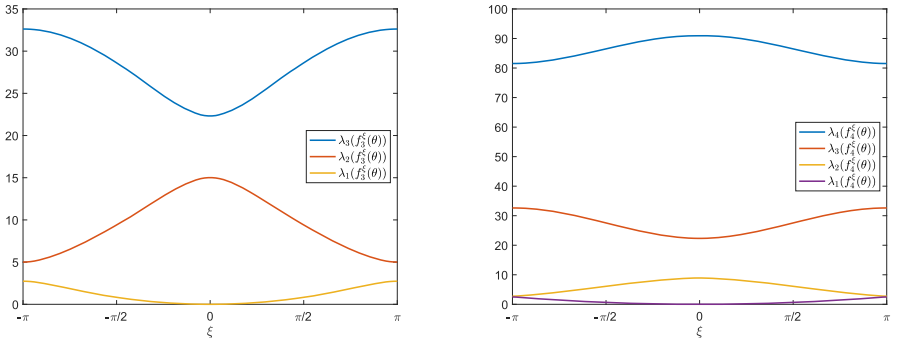

Fig. 6 A plot of the eigenvalue functions of the symbol for $\xi = 0.45$. The cases $r = 3$ (left) and $r = 4$ (right) are depicted

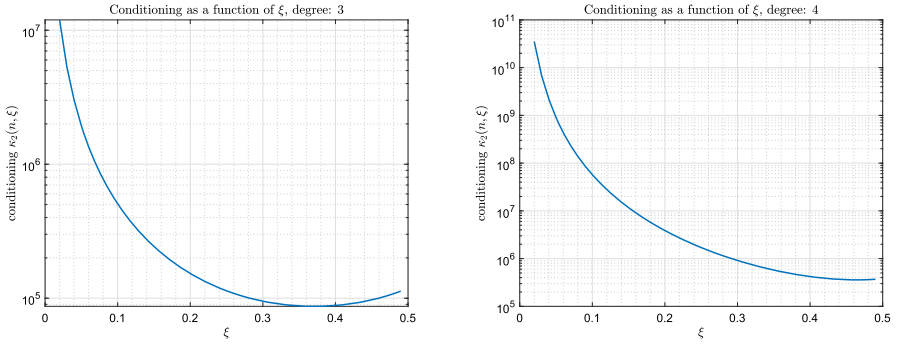

Fig. 7 A plot of the conditioning $\kappa_2(n, \xi)$ as ξ varies, in logarithmic scale. Parameters are as in the example of Figure 5. The cases $r = 3$ (left) and $r = 4$ (right) are depicted

to parametrize both cases via a single parameter ξ. When $r = 3$, interior supports become $s_2 = [1/2 - \xi, 1/2]$ and $s_3 = [1/2, 1/2 + \xi]$. Likewise, when $r = 4$, one adds the midpoint $s_3 = \xi_3 = \{1/2\}$ of $\widehat{I}$ (and relabels the former s_3 as s_4).

An example of the eigenvalue functions associated with the symbol of segmental continuous elements is depicted in Figure 6, where such functions are depicted for the parameter $\xi = 0.45$. The shape of the eigenvalues functions is close to that of the nodal case, although in this case ξ simply denotes a bound for the localization of the zeros of the corresponding Lagrange functions. Then, in Figure 7, we reproduce the experiment of Figure 5, looking for a parameter ξ that optimizes the conditioning. The segmental case $k = 1$ shows a peculiar behavior, if compared with the nodal case $k = 0$. While the magnitude of the conditioning is comparable between the two cases (match the panels of Figure 5 with those of Figure 7), only in the case $r = 3$ one observes an evident minimum for the conditioning. In the case $r = 4$, this quantity approaches a plateau around a stable level around $\xi = 0.5$. Notice that, even if $\xi = 0.5$, the associated Vandermonde matrix V is invertible, due to Lemma 1. This marks a sensible difference with the nodal case, and is again attributable to the non-constructiveness of the mean value theorem.

4.2 Non-constant coefficients

Recall that in the case $b(x) = 1$ the stiffness matrix A_n is a principal submatrix of size $nr - 1$ of the Toeplitz matrix $T_n(f_r^\xi)$ with generating function f_r^ξ defined in (18). For making sizes compatible, consider $\hat{A}_n(b) = \text{diag}(A_n(b), 1)$, $\text{order}(\hat{A}_n(b)) = nr$, with $A_n(b)$ being the stiffness matrix. The key observation is that

$$\hat{A}_n(b) = D_n([\sqrt{b}\,]I_r)T_n(f_\xi^r)D_n([\sqrt{b}\,]I_r) + E_{\xi,n}^{r,b},$$

where $D_n([\sqrt{b}\,]I_r)$ is a diagonal matrix composed by blocks that are multiple of the $r \times r$ identity matrix; it is understood that in the i-th block the function $b(x)$ is evaluated at the midpoint of the i-th element.

By direct inspection, axiom **GLT3**, item 3, in [14, Chapter 5, pp. 85-86] and Theorem 4 in A.2, we deduce that $\{E_{\xi,n}^{r,b}\}_n \sim_{\text{GLT}} 0$. Now, by axiom **GLT3**, items 1, 2 [14, Chapter 5, pp. 85-86], we know that $\{T_n(f_r^\xi)\}_n \sim_{\text{GLT}} f_r^\xi(\theta)$ and $\{D_n([\sqrt{b}\,]I_r)\}_n \sim_{\text{GLT}} [\sqrt{b(x)}\,]I_r$. Therefore the GLT symbol of $\{\hat{A}_n(b)\}_n$ is the Hermitian valued function defined as

$$\begin{aligned} f_{r,b}^\xi : \quad \Omega \times [-\pi, \pi] &\to \mathbb{C}^{r\times r} \\ (x, \theta) &\mapsto b(x) f_r^\xi(\theta), \end{aligned} \tag{28}$$

so that $\{\hat{A}_n(b)\}_n \sim_\lambda f_{r,b}^\xi$ and the same is true for $\{A_n(b)\}_n$ (see Theorem 3 in the Appendix).

4.3 Non-uniform grids

If Ω is partitioned into a uniform collection of elements $\mathcal{T}$, we may construct a non-uniform mesh by applying a sufficiently regular and invertible mapping $g : \Omega \to \Omega$. The resulting mesh is called *graded* [16]. When the domain $\Omega = I$ is one-dimensional, g simply transforms nodes as $y_k = g(x_k)$, being x_k the k-th node of the uniform mesh, fixing the endpoints of I.

From the point of view of our analysis, this is a particular case of non-constant coefficients, see [13, Theorem 6.17]. In fact, by applying the change of variables $y = g(x)$, it can be seen that discretizing a problem with diffusion coefficient $b(x)$ on the non-uniform mesh is equivalent to discretizing on an equispaced mesh the elliptic problem with coefficient

$$\tilde{b}(x) = \frac{b(g(x))}{g'(x)}. \tag{29}$$

The corresponding symbol of the sequence of stiffness matrices can thus be obtained by replacing b with $\tilde{b}$ in (28).

If the mesh is not graded, the present theory cannot be used as it is. Nevertheless, in the numerical section we show that the predictions of the conditioning and the proposed preconditioners behave quite robustly under random mesh perturbations, see Figure 13.

5 Numerical experiments

Following the derivations in Section 3, we know that the stiffness matrix has a tridiagonal Toeplitz-like structure with blocks of size r. The related generating function, given in Eq. (18) or Eq. (28), is a Hermitian-valued, positive semidefininte linear trigonometric polynomial, whose minimal eigenvalue has a unique zero at zero of order 2. Hence by exploiting known results in the literature [57], as indicated in Remark 8, we know that the conditioning grows as $c_r^\xi n^2$ where the constant c_r^ξ depends essentially on two analytic computable quantities, i.e. $\max_\theta \lambda_{\max}(f_r^\xi(\theta))$ and the second derivative of $\lambda_{\min}(f_r^\xi(\theta))$ at $\theta = 0$, according to Theorem 2. Figure 5 shows that the quantity can be affected by the constant c_r^ξ and that it can be minimized. Two basic techniques can hence be proposed for the numerical solution of the linear system:

a1. A preconditioned conjugate gradient (PCG) method where the preconditioner is a block circulant matrix with Strang correction having the same GLT symbol as the original matrix-sequence. For variable coefficient diffusion problems, the preconditioner is enriched with the use of block diagonal sampling matrix, as detailed below. The GLT symbol of the preconditioning matrix-sequence coincides with that of the original matrix-sequence and hence by axiom **GLT1** and items 3, 4 of axiom **GLT4** in [14, Chapter 5, pp. 85-86], we deduce that the preconditioned matrix-sequence has symbol 1, the latter meaning that all the eigenvalues are clustered at 1, according to Definition 3 and Remark 15, so indicating a fast convergence.

a2. A multigrid method which is essentially standard with a tensorization of the standard projection matrix. This is based on the inequality $L_n \le cT_n$ with $L_n = \Delta_n \otimes I_r$ and Δ_n being the standard discrete Laplacian obtained using centered Finite Differences i.e. $\Delta_n = T_n(g(\theta))$, $g(\theta) = 2 - 2\cos(\theta)$).

The preconditioner. We follow the approach a1 and propose a circulant preconditioner matrix, which can be applied efficiently via fast Fourier transforms (FFT). In particular, we use a r-block circulant preconditioner of size nr; since our stiffness matrix A_n has size $nr - 1$, we change the linear system by adding a fictitious equation so that the resulting coefficient matrix is

$$\hat{A}_n = \mathrm{diag}(A_n, 1), \quad \mathrm{order}(\hat{A}_n) = nr.$$

The circulant preconditioner for the $b(x) = 1$ case is then constructed as $S_n = C_n(f_r^\xi) + \frac{i}{nr}\mathbf{1}\mathbf{1}^T$, since $C_n(f_r^\xi)$ is singular with nullity 1 generated by the vector $\mathbf{1}$: the matrix S_n is known as the corrected Strang preconditioner of the Toeplitz matrix $T_n(f_r^\xi)$ (see [51] and references therein). Notice that $S_n = \hat{A}_n + R_n$ where all the matrices are real symmetric (hence Hermitian) and $\mathrm{rank}(R_n) \le 2r + 2$. Therefore by axiom **GLT3**, item 3, in [14, Chapter 5, pp. 85-86] and using the first part of Theorem 4, we deduce that $\{R_n\}_n \sim_{\mathrm{GLT}} 0$ so that by axiom **GLT3**, item 3, in [14, Chapter 5, pp. 85-86] the three matrix-sequences $\{T_n(f_r^\xi)\}_n$, $\{\hat{A}_n\}_n$, $\{S_n\}_n$ have the same GLT symbol f_r^ξ. Therefore, by exploiting axiom **GLT4**, items 3, 4, in [14, Chapter 5, pp. 85-86] we easily conclude that the preconditioned matrix-sequence has GLT symbol

Table 1 Approximation error and convergence rate for $r = 3$, for all elements presented

	Interpolation				Histopolation	
$\mathbf{r = 3}$	error		Convergence rate		Error	Convergence rate
Elements	Lagrangian	Weights	Lagrangian	Weights	$\xi = 0.37$	
10	5.26×10^{-4}	5.26×10^{-4}			5.26×10^{-4}	
20	6.58×10^{-5}	6.58×10^{-5}	2.9991	2.9991	6.58×10^{-5}	2.9991
40	8.22×10^{-6}	8.22×10^{-6}	2.9998	2.9998	8.22×10^{-6}	2.9998
80	1.03×10^{-6}	1.03×10^{-6}	2.9999	2.9999	1.03×10^{-6}	2.9999
160	1.29×10^{-7}	1.31×10^{-7}	3.0000	2.9640	1.29×10^{-7}	3.0000
320	1.73×10^{-8}	1.61×10^{-8}	2.8932	3.0361	1.61×10^{-8}	2.9999
640	2.02×10^{-9}	2.02×10^{-9}	3.0982	2.9932	2.20×10^{-9}	2.8707
1280	6.80×10^{-10}	1.23×10^{-9}	1.5705	0.7160	4.10×10^{-9}	−0.9016

equal to 1 and hence it is weakly clustered at 1 in a spectral sense. Indeed in this specific setting more is known since the preconditioned matrix minus the identity has rank bounded by $2r - 2$ and hence a constant number of iterations has to be expected.

5.1 Convergence of the FEM method

First of all, we check that the convergence of the FEM Galerkin discretization is in accordance with the theory. We show this for the case of constant coefficients and consider a uniform mesh. It is well known that, if the datum f is sufficiently regular, the H^1-approximation error given by the finite element method for this kind of problems decays as h^r, being h the element size and r the polynomial degree (see, e.g., [27]). Since this is a Galerkin method, the error shall not depend on the projector but only on the discrete space in which the solution is sought. As a consequence, we check that the convergence for equidistributed Lagrangian and weights coincide, since in both cases they seek for a solution in the subspace of functions in H^1 which are locally polynomials of degree r in each element. Table 1 (for $r = 3$) and Table 2 (for $r = 4$) show that the theoretical convergence order is attained both for usual nodal finite elements and segmental ones, at least until computations start being affected by rounding errors.

5.2 Constant coefficients

We compare the spectrum of the Laplace operator with the symbol derived in the preceding sections. Figure 8 reports, for $r = 3$ and coefficient $b(x) \equiv 1$, a comparison between the spectrum of the exact operator (blue, dashed line) and the spectral symbol (solid lines of different colors: as the number of elements increases, the color of the corresponding solid line changes). Even with a very small number of elements (e.g., when $N_{\text{el}} = 4$), the exact spectrum and the symbol are in practice overlapped. This is in accordance with the theory of Section 3. Moreover, we see that r distinct branches

Table 2 Approximation error and convergence rate for $r = 4$, for all elements presented

	Interpolation				Histopolation	
$\mathbf{r = 4}$	Error		Convergence rate		Error	Convergence rate
elements	Lagrangian	Weights	Lagrangian	Weights	$\xi = 0.40$	
2	5.72×10^{-3}	5.72×10^{-3}			5.72×10^{-3}	
4	3.58×10^{-4}	3.58×10^{-4}	3.9993	3.9993	3.58×10^{-4}	3.9993
8	2.25×10^{-5}	2.25×10^{-5}	3.9931	3.9931	2.25×10^{-5}	3.9931
16	1.41×10^{-6}	1.41×10^{-6}	3.9980	3.9966	1.41×10^{-6}	3.9980
32	8.79×10^{-8}	1.17×10^{-7}	3.9995	3.5856	8.79×10^{-8}	3.9995
64	9.74×10^{-9}	1.37×10^{-8}	3.1738	3.0959	5.50×10^{-9}	3.9998
128	3.57×10^{-10}	3.53×10^{-10}	4.7704	5.2782	3.71×10^{-10}	3.8903
256	3.58×10^{-10}	3.39×10^{-10}	−0.0046	0.0611	3.87×10^{-10}	−0.0625

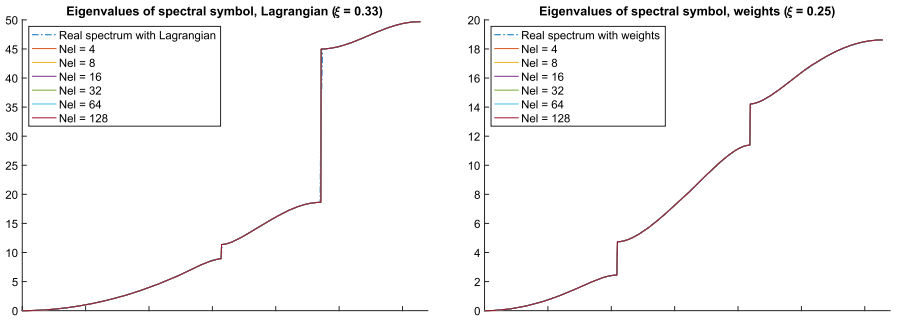

Fig. 8 A plot of the spectrum of the Laplacian with constant coefficients. The dashed line, which represents the continuous spectrum, is overlapped by the solid lines that represent the symbol associated with different mesh sizes. Lagrange equispaced elements (left) and optimized weights (right) are compared. The degree $r = 3$ is depicted

are present. The latter holds both for the case of equispaced Lagrangian (left) and optimized weights (right). Notice that the magnitude of the eigenvalues changes. The case $r = 4$ (not shown) is analogous.

We then report, in Table 3, the conditioning of the stiffness matrices and the number of iterations required by conjugate gradients for solving the system when the circulant preconditioner is applied. We observe that our preconditioning strategy is optimal in all cases as the number of iterations quickly stabilizes. In fact, the spectra of the preconditioned matrices in Figure 9 show that the considered circulant preconditioner induces a strong eigenvalue clustering around 1 in both cases. Also the number and size of the outliers coincide.

5.3 Non-constant coefficients

In this section we repeat the same analysis done in Section 5.2, in the case of a non-constant coefficient $b(x)$. For the sake of simplicity, we present an example in

Table 3 Comparison of the conditioning of the stiffness matrix and number of iterations needed by conjugate gradients after preconditioning via circulant matrices for $r = 3$ (above) and $r = 4$ (below)

$\mathbf{r = 3}$	Conditioning		Iterations	
Elements	Lagrangian	Weights	Lagrangian	Weights
10	9.11×10^2	7.75×10^2	4	4
20	3.65×10^3	3.10×10^3	4	4
40	1.46×10^4	1.24×10^4	4	4
80	5.83×10^4	4.96×10^4	5	5
160	2.33×10^5	1.98×10^5	5	5
320	9.33×10^5	7.93×10^5	6	6
640	3.73×10^6	3.17×10^6	6	6
1280	1.49×10^7	1.27×10^7	6	6
$\mathbf{r = 4}$	Conditioning		Iterations	
Elements	Lagrangian	Weights	Lagrangian	Weights
2	1.14×10^2	9.06×10^1	4	4
4	4.81×10^2	3.71×10^2	4	4
8	1.92×10^3	1.48×10^3	4	4
16	7.70×10^3	5.94×10^3	4	4
32	3.08×10^4	2.38×10^4	4	4
64	1.23×10^5	9.50×10^4	5	5
128	4.93×10^5	3.80×10^5	5	6
256	1.97×10^6	1.52×10^6	6	6

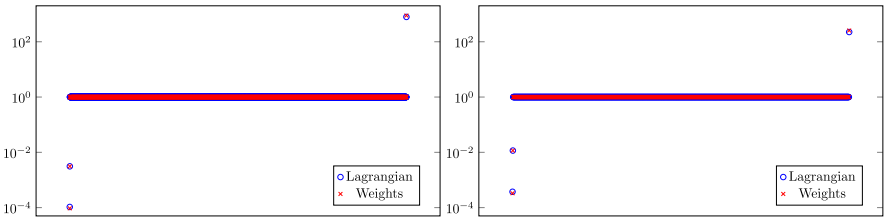

Fig. 9 Spectrum of the preconditioned stiffness matrix for Lagrangian and weights. Degrees $r = 3$ (left) with $N = 80$ elements and $r = 4$ (right) with $N = 64$ elements are shown

which $b(x) = 1 + x^2$. It is here worth pointing out that the positivity of b is required for the well-posedness, although GLT theory applies in the case of a function $b(x)$ Riemann integrable over its definition domain. Figure 10 shows that, also in this case, the spectrum is captured by the spectral symbol.

Clearly, non-constant coefficients make it harder to construct an ad hoc preconditioner via Toeplitz or circulant matrices, since elements do not scale only by a constant but accordingly to the coefficient $b(x)$ as well. Here we consider the diagonal plus cir-

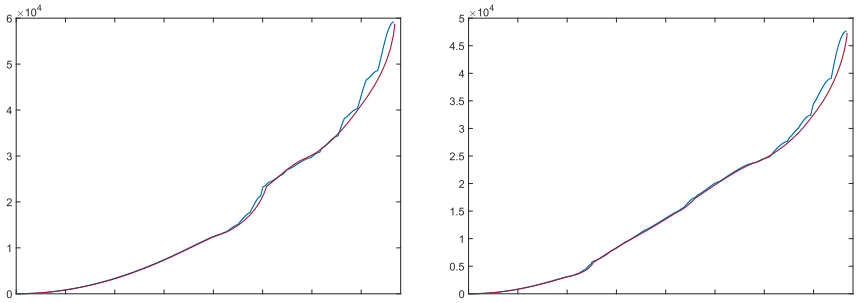

Fig. 10 Spectrum of the operator (red) vs spectrum of the symbol (blue), in the case of non-constant coefficients with $a(x) = 1 + x^2$. Degree 3 with $N = 1280$ elements is represented. Results for $r = 4$ are comparable (color figure online)

culant preconditioner with Strang correction based on the symbol $f^{\xi}_{r,b}(x, \theta)$ described at the beginning of this section, which is defined as

$$P_n(b) = D_n([\sqrt{b}\,]I_r)S_n D_n([\sqrt{b}\,]I_r). \tag{30}$$

By following the very same reasoning as before, we infer that $\{\hat{A}_n(a)\}_n$ and $\{P_n(a)\}_n$ have the same GLT symbol $f^{r,a}_{\xi}$. Therefore, by exploiting axiom **GLT4**, items 3, 4, in [14, Chapter 5, pp. 85-86], we easily conclude that the preconditioned matrix-sequence has GLT symbol equal to 1 and hence it is weakly clustered at 1 in a spectral sense, the latter being an indication that the related preconditioned conjugate gradient is effective.

Table 4 reports the performance of the preconditioned conjugated gradient for the degree $r = 3$ and $r = 4$. In both cases the number of iterations quickly stabilizes. The spectra of the preconditioned matrices for the cases $r = 3$ and $r = 4$ are qualitatively almost identical. In Figure 11 we plot the case $r = 3$. From the left panel one can appreciate the presence of a cluster at 1 and of three outliers, as in the constant coefficient case. The right panel, using a linear scale on the vertical axis, shows the slight spreading of the eigenvalues in the cluster. This motivates the increment in the number of iterations with respect to the constant coefficients case discussed in Section 5.2.

5.4 Graded mesh

In order to better detect the effect of the mesh mapping, we consider the elliptic problem with unit diffusion coefficient. According to (29), this is equivalent to considering a problem with a variable coefficient $\widetilde{b}(x)$, which is a function of the mesh mapping $g(x)$, on a uniform mesh. Following the remarks in Section 4.3, a preconditioner for the case of graded meshes can be obtained by setting $b(x) = \frac{1}{g'(x)}$ in (30).

In particular, we choose the mesh mapping $g(x) = ce^x + k$, with c, k such that $g(0) = 0$ and $g(1) = 1$. Results are in accordance with the non-constant coefficient

Table 4 Comparison of the conditioning of the stiffness matrix and number of iterations needed by conjugate gradients after preconditioning via circulant matrices for $r = 3, 4$. Non-constant coefficient

r = 3	Conditioning		Iterations	
Elements	Lagrangian	Weights	Lagrangian	Weights
10	1.22×10^3	1.05×10^3	11	11
20	5.14×10^3	4.43×10^3	12	12
40	2.13×10^4	1.82×10^4	12	12
80	8.66×10^4	7.36×10^4	12	13
160	3.49×10^5	2.96×10^5	14	14
320	1.40×10^6	1.19×10^6	15	15
640	5.63×10^6	4.78×10^6	16	16
1280	2.25×10^7	1.91×10^7	16	17
r = 4	Conditioning		Iterations	
Elements	Lagrangian	Weights	Lagrangian	Weights
2	1.34×10^2	8.56×10^1	8	8
4	6.05×10^2	4.29×10^2	11	11
8	2.58×10^3	1.95×10^3	12	12
16	1.07×10^4	8.33×10^3	12	12
32	4.44×10^4	3.44×10^4	13	13
64	1.82×10^5	1.40×10^5	14	15
128	7.36×10^5	5.65×10^5	15	15
256	2.96×10^6	2.28×10^6	15	15

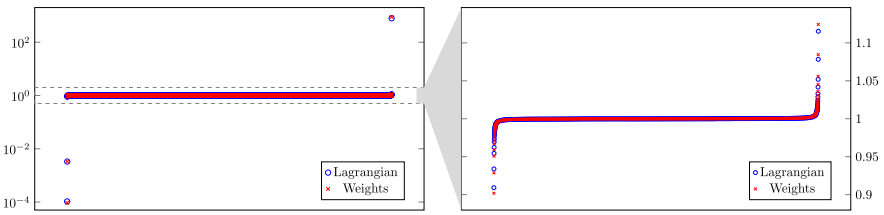

Fig. 11 Spectrum of the preconditioned stiffness matrix for Lagrangian and weights for the non-constant coefficients case. Degree $r = 3$ with $N = 80$ elements is depicted. On the right the same data, except the 3 outliers, are plotted with linear scale on the vertical axis

case. The spectrum of the preconditioned matrix for $r = 3$ is depicted in Figure 12, which shows that eigenvalues appear to be again weakly clustered around 1, with the presence of the three outliers. In this case the amplitude of the interval is slightly larger, approximately [0.85, 1.15]. A comparable situation holds for $r = 4$. Iteration counts are reported in Table 5, and are in fact close to the case of non-constant coefficients.

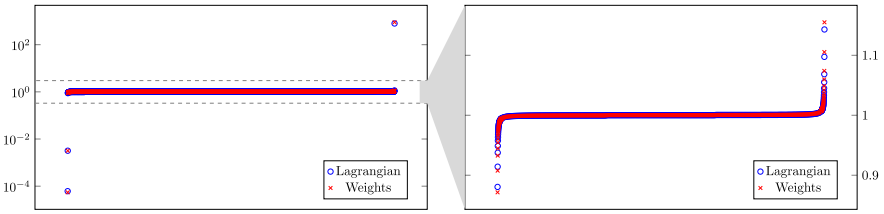

Fig. 12 Spectrum of the preconditioned stiffness matrix for Lagrangian and weights-based elements for the non-constant coefficients case. Degree $r = 3$ with $N = 80$ elements is depicted. On the right the same data, except the 3 outliers, are plotted with linear scale on the vertical axis

Table 5 Iterations needed by conjugate gradients after preconditioning via circulant matrices for $r = 3, 4$. Graded mesh

r = 3			**r = 4**		
	Iterations			Iterations	
Elements	Lagrangian	Weights	Elements	Lagrangian	Weights
10	12	12	2	8	8
20	12	12	4	12	12
40	13	13	8	12	13
80	13	15	16	13	13
160	15	15	32	13	15
320	15	16	64	15	15
640	17	17	128	16	16
1280	18	18	256	16	18

5.5 Robustness of the preconditioner

To test the robustness of the preconditioner we perform two different numerical tests. In the first we remove the hypothesis of uniformity or gradedness of the mesh. In the second we analyse how the preconditioner is affected by the selection of the localisation parameter ξ.

Random mesh. We introduce in the mesh generator a randomness parameter θ. The randomisation of the mesh is obtained as follows. First, we compute a uniform partitioning of I and store the endpoints of the segments increasingly

$$0 = \xi_0 < \xi_1 < \ldots < \xi_n = 1$$

with $\xi_j = \frac{j}{n}$. Thus every segment $I_j \doteq [\xi_{j-1}, \xi_j]$ has length $|I_j| = \frac{j+1-j}{n} = \frac{1}{n}$. For each $j = 1, \ldots, n-1$ we create a random coefficient $c_j \in \left(-\frac{1}{2n}, \frac{1}{2n}\right)$ and replace ξ_j with $\xi_i' = \xi_j + \theta c_j$. By construction, we obtain a sequence

$$0 = \xi_0' \doteq \xi_0 < \xi_1' < \ldots < \xi_n' \doteq \xi_n = 1$$

and the randomised mesh is thus that whose j-th element is $I_j' = [\xi_{j-1}', \xi_j']$.

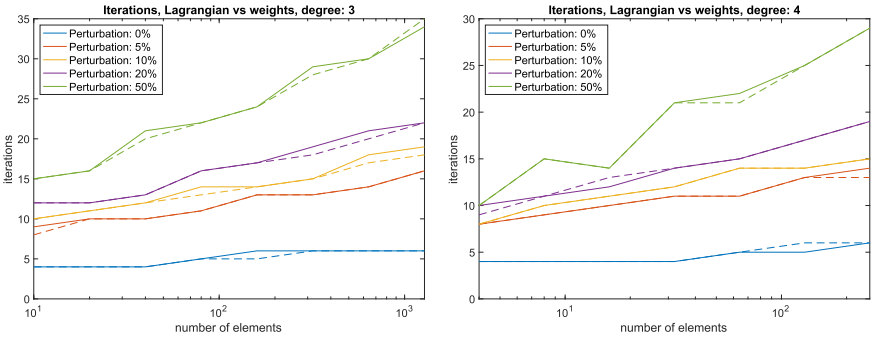

Fig. 13 Randomised mesh. A comparison between equispaced Lagrangian and optimized weights in terms of PCG iterations for degrees $r = 3$ (left) and $r = 4$ (right). To same color corresponds the same entity of perturbation. Dashed lines represent equidistributed Lagrangian whereas solid lines represent optimized weights. As θ grows, the corresponding line ascends (color figure online)

Clearly the analysis developed for the uniform case does not apply directly, as measures $|I'_j|$'s may sensibly vary when increasing the parameter θ. To estimate the robustness of our preconditioning strategy, we use the circulant preconditioner built on the symbol f_ξ^r associated with the uniform mesh case (that is, as if the randomness parameter was set to $\theta = 0$). We compare the iterations of the PCG as the parameter θ varies. In particular, we choose θ increasing from 0.05 to 0.5, see Figure 13. In all cases, we observe a mild increase in the iteration count as the mesh size increases. The scale of the horizontal axis is logarithmic, so that it is easily appreciable that this dependence is of type $d\log(n)$, for d a proper constant; this behavior could indicate that the minimal outlier may tend to zero as $n^{-\alpha}$, $\alpha \geq 2$. In any case, we point out that the increase in iterations is very mild up to $\theta = 0.2$.

Robustness with respect to ξ. Finally, we consider the robustness of our preconditioning strategy as a function of the parameter ξ. We consider the case of non-constant coefficients (see Section 5.3) with $N = 40$ elements for $r = 3$ and $N = 32$ elements for $r = 4$. This choice yields comparable size stiffness matrices. Figure 14 depicts the spectrum of the preconditioned stiffness matrix, leaving out the unique largest outlier. In all cases, eigenvalues cluster on a relatively small interval, whose size is larger for small ξ and quickly decreases as the parameter ξ approaches the optimal value and overcome the Lagrangian case $\xi = 1/r$. The order of magnitude of the largest outlier ranges between 10^1 and 10^2. The bottom part of the graphs shows the number of PCG iterations, that are well correlated with the spread of the preconditioned spectrum.

Recall the condition numbers shown in Figure 5. We observed that $\kappa_2(n, \xi)$ increases when ξ approaches both 0 and $1/2$, consistently with the loss of the unisolvence at these extreme values of the parameter. Figure 14 shows that our preconditioning strategy grants a constant iteration counts in a range $\xi \in [0.25, 0.45]$ and a mild increase as $\xi \approx 0.1$. When ξ tends to the extrema of the interval, the preconditioning handles the case $\xi \approx 1/2$ much better than the case $\xi \approx 0$. A possible explanation of this fact may follow from Remark 11.

Remark 14 In the present setting, since the structures are banded, direct methods such as the Gaussian elimination may be applied. However, in the multi-dimensional

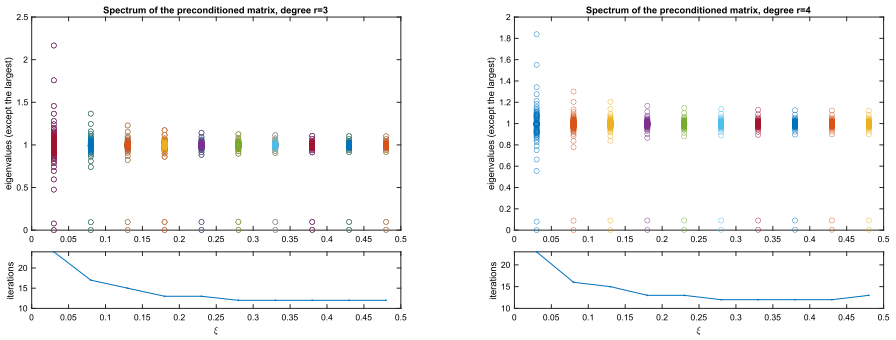

Fig. 14 Spectrum of the preconditioned stiffness matrix and number of PCG iterations as a function of the ξ parameter. Case $r = 3$, $N = 40$ (left) and $r = 4$, $N = 32$ (right). For graphical purposes, the largest eigenvalue has been omitted in all cases

case, the fill-in destroys the computational optimality of direct solvers, while our preconditioning strategy can be adapted for $d \geq 2$. In this case, a theoretical obstruction emerges (see [59, 62, 63]) and it is impossible in general to obtain a strong clustering for the preconditioned matrix-sequence, when either a circulant or a general matrix algebra preconditioning is employed. Nevertheless, it is possible to overcome the problem, also in the variable coefficient setting, by combining e.g. (circulant) preconditioning in the Krylov methods and multigrid strategies in the spirit of the multi-iterative solvers, see [29, 30] and references therein.

6 Conclusions

In this work we analysed weights-based finite elements applied to the one-dimensional Laplace equation, both with constant and non-constant coefficients. In this context, we studied two different discretizations of the problem which stem from weights. The first one gives the usual nodal Lagrange elements, whereas the second is associated with the problem of histopolation of univariate functions. In both cases, such elements depend on a localization parameter ξ and contain, in an appropriate sense, the well-known equidistributed Lagrange finite elements.

Main results. Exploiting the GLT theory, we provided a detailed analysis of the conditioning of the problem and a thorough spectral analysis of the matrix-sequence by emphasizing the spectral distribution in the Weyl sense, including the branch analysis and the clustering. While the shape and the clustering of the spectrum of the matrix of the system are qualitatively constant, this analysis demonstrated that the conditioning of the problem, compatibly with the nature of the problem, is in fact dependent on the parameter ξ. The sensitivity to this parameter varies between the case of the nodal ($k = 0$) and the segmental ($k = 1$) discretization. As this analysis requires a good understanding of the cardinal functions of polynomial spaces where the approximate solution is sought, we proved some results on cardinal bases associated with histopolation. This is needed to handle the case $k = 1$.

We thus proposed a preconditioning strategy for the solution of the linear system associated with the finite element problem. This preconditioner is based on a circulant matrix, so that FFT algorithms may be applied. We then carried several numerical experiments, all based on a PCG method, that evidenced that the behavior for different parameters ξ's is comparable, in terms of clustering of the preconditioned matrix and hence of iterations, as long as the conditioning of the matrix of the system does not explode. In contrast, when the Vandermonde matrix approaches rank-deficiency, the spectrum of the preconditioned matrix spreads and the number of iterations increases.

Novelty of the paper. The present contribution is the first in analyzing in depth the spectral features of the matrices and matrix-sequences arising in weights-based finite element exterior calculus by using Toeplitz and GLT technology, albeit most results are limited to the continuous one-dimensional setting. To the best of the authors' knowledge, the interpolation theory developed for treating the normalized segmental case ($k = 1$) is also new, and expands results on histopolation of functions.

Outlook on future research. Because of the very general definition of weights in terms of differential forms, the theory developed can be extended to cover the case of both univariate discontinuous and multivariate finite element approximation, which we set as two feasible and promising directions to pursue. For what concerns discontinuous elements, the main obstacles been discussed in Section 2.2, and concern the replicability of some technical lemmas regarding Lagrange functions. In view of the computations performed in the aforementioned section, we reckon that appropriate geometrical assumptions on the supports of the dofs can solve the impasse. Likely, the structure of the corresponding symbol changes, due to the coupling introduced by jump and cut functions, but GLT theory already proved to be able to handle such a situation.

The multi-dimensional case is widely known to be a relevant topic (see, e.g., [2] for a valuable perspective on this problem for Nédélec elements). It carries some obstructions too. First of all, the coordinate representation of the Hodge Laplacian gives a larger variety of operators (gradient, curl, divergence, ecc.) acting on differential forms. To the state of the art, the interpolation theory for polynomial differential forms has some gaps, and the corresponding Lagrange functions can only be implicitly computed by inverting the matrix defined in Eq. (5). Exploiting Proposition 1, one may then invoke the spectral multilevel block Toeplitz [66, 67] and the spectral multilevel block GLT tools, that are available in such a setting [12, 13, 34]. In contrast, preconditioning alone is hardly effective alone in the multidimensional case. This is due to the theoretical barriers proved in [59, 62, 63]. Consequently, as discussed in Remark 14, we expect that a multi-iterative approach has to be considered [29, 30]. Following such references, we point out that the there considered multi-iterative solvers for multi-dimensional problems are based on a deep analysis of the corresponding one-dimensional case.

A Spectral tools and useful matrix structures

When the number n of elements in the mesh increases, the size of the linear system also increases, together with its conditioning. We are concerned with the spectral

analysis of the matrix structures and the design of appropriate preconditioners for Krylov methods, with the idea of obtaining robustness and optimality with respect to the relevant parameters. Our tools come from block Toeplitz operators and block GLT matrix-sequences. To this end, in Section A.1 we introduce the notion of distribution in the Weyl sense and clustering, when a general matrix-sequence is considered. Section A.2 is devoted to block Toeplitz, circulant, sampling diagonal matrices, while Section A.3 shortly introduces the $*$-algebra of GLT sequences.

A.1 Clustering and distribution

We begin with the notion of distribution in the Weyl sense, when a matrix-valued symbol occurs, both in the sense of the eigenvalues and singular values. The notion of clustering at a given fixed point, both in the sense of eigenvalues and singular values, can be seen as a special case of the distribution notions.

• **Sequences of Matrices and Block Matrix-Sequences.** A sequence of matrices is any sequence of the form $\{A_n\}_n$, where A_n is a square matrix of size d_n, d_n is monotonically strictly increasing so that $d_n \to \infty$ as $n \to \infty$. Let $r \geq 1$ be a fixed positive integer independent of n. A r-block matrix-sequence - or simply a matrix-sequence if r can be inferred from the context or we do not need/want to specify it - is a special sequence of matrices $\{A_n\}_n$ in which the size of A_n is $d_n = r\phi_n$, with $\{\phi_n\}_n$ being a strictly increasing sequence of positive integers. In the following sections, A_n is the stiffness matrix (11) obtained when partitioning the domain into n elements.

• **Singular Value and Eigenvalue Distribution of a Sequence of Matrices.** Let μ_t be the Lebesgue measure in $\mathbb{R}^t$, $t \geq 1$. Throughout the current work, all the terminology from measure theory (such as "measurable set", "measurable function", "a.e.", etc.) is referred to the Lebesgue measure. A matrix-valued function $f : D \subseteq \mathbb{R}^t \to \mathbb{C}^{r\times r}$ is said to be measurable (resp., continuous, Riemann-integrable, in $L^p(D)$, etc.) if its components $f_{\alpha\beta} : D \to \mathbb{C}$, $\alpha, \beta = 1, \ldots, r$, are measurable (resp., continuous, Riemann-integrable, in $L^p(D)$, etc.). We denote by $C_c(\mathbb{R})$ (resp., $C_c(\mathbb{C})$) the space of continuous complex-valued functions with bounded support defined on $\mathbb{R}$ (resp., $\mathbb{C}$). If $A \in \mathbb{C}^{m\times m}$, the singular values and the eigenvalues of A are denoted by $\sigma_1(A), \ldots, \sigma_m(A)$ and $\lambda_1(A), \ldots, \lambda_m(A)$, respectively.

Definition 2 Let $\{A_n\}_n$ be a sequence of matrices, with A_n of size d_n, and let $f : D \subset \mathbb{R}^t \to \mathbb{C}^{r\times r}$ be a measurable function defined on a set D with $0 < \mu_t(D) < \infty$.

– We say that $\{A_n\}_n$ has a (asymptotic) singular value distribution described by f, and we write $\{A_n\}_n \sim_\sigma f$, if

$$\lim_{n\to\infty} \frac{1}{d_n} \sum_{i=1}^{d_n} F(\sigma_i(A_n)) = \frac{1}{\mu_t(D)} \int_D \frac{\sum_{i=1}^{r} F(\sigma_i(f(\mathbf{x})))}{r} \mathrm{d}\mathbf{x}, \qquad \forall\, F \in C_c(\mathbb{R}). \tag{31}$$

– We say that $\{A_n\}_n$ has a (asymptotic) spectral (or eigenvalue) distribution described by f, and we write $\{A_n\}_n \sim_\lambda f$, if

$$\lim_{n\to\infty}\frac{1}{d_n}\sum_{i=1}^{d_n}F(\lambda_i(A_n))=\frac{1}{\mu_t(D)}\int_D\frac{\sum_{i=1}^{r}F(\lambda_i(f(\mathbf{x})))}{r}\mathrm{d}\mathbf{x},\qquad\forall\,F\in C_c(\mathbb{C}). \tag{32}$$

If $\{A_n\}_n$ has both a singular value and an eigenvalue distribution described by f, we write $\{A_n\}_n\sim_{\sigma,\lambda}f$.

We remind that the notion contained in Definition 2 and the related information are useful in engineering applications [36], e.g. for the computation of the relevant vibrations, and in the analysis of the (asymptotic) convergence speed of iterative solvers for large linear systems or for improving the convergence rate by e.g. the design of appropriate preconditioners [15, 16].
The next theorem gives useful tools for computing the spectral distribution of sequences formed by Hermitian matrices. For the related proof, we refer the reader to [46, Theorem 4.3]. In what follows, the conjugate transpose of the matrix A is denoted by A^*. If $A\in\mathbb{C}^{m\times m}$ and $1\le p\le\infty$, we denote by $\|A\|_p$ the Schatten p-norm of A, i.e., the p-norm of the vector $(\sigma_1(A),\dots,\sigma_m(A))$. The Schatten ∞-norm $\|A\|_\infty$ is the largest singular value of A and coincides with the spectral norm $\|A\|$. The Schatten 1-norm $\|A\|_1$ is the sum of the singular values of A and is often referred to as the trace-norm of A. The Schatten 2-norm $\|A\|_2$ coincides with the Frobenius norm of A. Schatten p-norms are treated in detail in a beautiful book by Bhatia [18].

Theorem 3 *Let $\{X_n\}_n$ be a sequence of matrices, with X_n Hermitian of size d_n, and let $\{P_n\}_n$ be a sequence such that $P_n\in\mathbb{C}^{d_n\times\delta_n}$, $P_n^*P_n=I_{\delta_n}$, $\delta_n\le d_n$ and $\delta_n/d_n\to1$ as $n\to\infty$. Then, $\{X_n\}_n\sim_{\sigma,\lambda}f$ if and only if $\{P_n^*X_nP_n\}_n\sim_{\sigma,\lambda}f$.*

Now we turn to the definition of clustering. For $z\in\mathbb{C}$ and $\epsilon>0$, let $B(z,\epsilon)$ be the disk with center z and radius ϵ, $B(z,\epsilon)\doteq\{w\in\mathbb{C}:\,|w-z|<\epsilon\}$. For $S\subseteq\mathbb{C}$ and $\epsilon>0$, we denote by $B(S,\epsilon)$ the ϵ-expansion of S, defined as $B(S,\epsilon)\doteq\bigcup_{z\in S}B(z,\epsilon)$.

Definition 3 Let $\{X_n\}_n$ be a sequence of matrices, with X_n of size d_n tending to infinity, and let $S\subseteq\mathbb{C}$ be a nonempty closed subset of $\mathbb{C}$. $\{X_n\}_n$ is *strongly clustered* at S in the sense of the eigenvalues if, for each $\epsilon>0$, the number of eigenvalues of X_n outside $B(S,\epsilon)$ is bounded by a constant q_ϵ independent of n. In symbols,

$$q_\epsilon(n,S)\doteq\#\{j\in\{1,\dots,d_n\}:\lambda_j(X_n)\notin B(S,\epsilon)\}=O(1),\quad\text{as } n\to\infty.$$

$\{X_n\}_n$ is *weakly clustered* at S if, for each $\epsilon>0$,

$$q_\epsilon(n,S)=o(d_n),\quad\text{as } n\to\infty.$$

If $\{X_n\}_n$ is strongly or weakly clustered at S and S is not connected, then the connected components of S are called sub-clusters.

Remark 15 Recall that, for a measurable function $g:D\subseteq\mathbb{R}^t\to\mathbb{C}$, the essential range of g is defined as $\mathcal{ER}(g)\doteq\{z\in\mathbb{C}:\,\mu_t(\{g\in B(z,\epsilon)\})>0\text{ for all }\epsilon>0\}$, where $\{g\in B(z,\epsilon)\}\doteq\{x\in D:\,g(x)\in B(z,\epsilon)\}$. $\mathcal{ER}(g)$ is always closed; moreover,

if g is continuous and D is contained in the closure of its interior, then $\mathcal{ER}(g)$ coincides with the closure of the image of g.

Hence, if $\{X_n\}_n \sim_\lambda f$ (with $\{X_n\}_n$, f as in Definition 2), then, by [38, Theorem 4.2], $\{X_n\}_n$ is weakly clustered at the essential range of f, defined as the union of the essential ranges of the eigenvalue functions $\lambda_i(f)$, $i = 1, \ldots, r$: $\mathcal{ER}(f) \doteq \bigcup_{i=1}^{r} \mathcal{ER}(\lambda_i(f))$. Finally, if $\mathcal{ER}(f) = s$ with s fixed complex number and $\{X_n\}_n \sim_\lambda f$, then $\{X_n\}_n$ is weakly clustered at s. All the considerations above can be translated in the singular value setting as well, with obvious minimal modifications. For further relationships among distribution, clustering, Schatten p-norms the reader is referred to [58] (see also [67]).

A.2 Block Toeplitz/circulant/diagonal matrices and zero-distributed matrix-sequences

In this subsection we introduce three types of matrix structures. The first two have an algebraic definition for every fixed dimension (block Toeplitz/circulant matrices and block diagonal structures), while the last has only an asymptotic sense (zero-distributed matrix-sequences). As it is clarified in the sequel, starting from Subsection A.3, we deal with matrix-sequences consisting of these three matrix structures, especially when defining the basics of the theory of block GLT sequences.

• **Block Toeplitz/circulant Matrices.** We concisely summarize the definition and relevant properties of block Toeplitz matrices. Given r, n fixed positive integers i.e. given $r, n \in \mathbb{N}^+$, a matrix of the form $[A_{i-j}]_{i,j=1}^{n} \in \mathbb{C}^{nr \times nr}$ with blocks $A_k \in \mathbb{C}^{r \times r}$, $k = -(n-1), \ldots, n-1$, is called block Toeplitz matrix, or, more precisely, r-block Toeplitz matrix. Given a matrix-valued function $f : [-\pi, \pi] \to \mathbb{C}^{r \times r}$ belonging to $L^1([-\pi, \pi])$, we denote its Fourier coefficients by

$$\hat{f}_k = \frac{1}{2\pi} \int_{[-\pi,\pi]} f(\theta) e^{-\hat{i}\, k\theta}\, d\theta \in \mathbb{C}^{r \times r}, \quad k \in \mathbb{Z}. \tag{33}$$

For every $n \in \mathbb{N}^+$, the n-th Toeplitz matrix associated with f is defined as

$$T_n(f) \doteq [\hat{f}_{i-j}]_{i,j=1}^{n} \tag{34}$$

or, equivalently, as

$$T_n(f) = \sum_{|j|<n} J_n^{(j)} \otimes \hat{f}_j \tag{35}$$

where $\otimes$ denotes the (Kronecker) tensor product of matrices, while $J_m^{(l)}$ is the matrix of order m whose (i, j) entry equals 1 if $i - j = l$ and zero otherwise. We call $\{T_n(f)\}_{n \in \mathbb{N}^+}$ the family of (block) Toeplitz matrices associated with f, which, in turn, is called the generating function of $\{T_n(f)\}_{n \in \mathbb{N}^+}$. In perfect analogy we define block circulant matrices. Given $r, n \in \mathbb{N}^+$, a matrix of the form $[A_{(i-j) \bmod n}]_{i,j=1}^{n} \in \mathbb{C}^{nr \times nr}$ with blocks $A_k \in \mathbb{C}^{r \times r}$, $k = 0, \ldots, n-1$, is called block circulant matrix, or, more precisely, r-block circulant matrix. The n-th circulant matrix associated with f is

defined as $C_n(f) \doteq \sum_{|j|<n/2} Z_n^{(j)} \otimes \hat{f}_j$ where $Z_m^{(l)} = [Z_m^{(1)}]^l$ is the matrix of order m whose (i, j) entry equals 1 if $(i - j) \bmod m = l$ and zero otherwise.

• **Block Diagonal Sampling Matrices.** For $n \in \mathbb{N}^+$, $d = 1$, and $a : [0, 1] \to \mathbb{C}^{r\times r}$, we define the block diagonal sampling matrix $D_n(a)$ as the block diagonal matrix

$$D_n(a) \doteq \text{diag}_{i=1,\ldots,n} a\Big(\frac{i}{n}\Big) = \begin{bmatrix} a(\frac{1}{n}) & & & \\ & a(\frac{2}{n}) & & \\ & & \ddots & \\ & & & a(1) \end{bmatrix} \in \mathbb{C}^{rn\times rn}.$$

• **Zero-Distributed Sequences.** A sequence of matrices $\{Z_n\}_n$ such that $\{Z_n\}_n \sim_\sigma 0$ is referred to as a zero-distributed sequence. Note that, for any $r \geq 1$, $\{Z_n\}_n \sim_\sigma 0$ is equivalent to $\{Z_n\}_n \sim_\sigma O_r$ (throughout this paper, O_m and I_m denote the $m \times m$ zero matrix and the $m \times m$ identity matrix, respectively). Theorem 4 provides an important characterization of zero-distributed sequences together with a useful sufficient condition for detecting such sequences [58]. Throughout this paper we use the natural convention $1/\infty = 0$.

Theorem 4 *Let $\{Z_n\}_n$ be a sequence of matrices, with Z_n of size d_n, and let $\|\cdot\|$ be the spectral norm. Then*

- *$\{Z_n\}_n$ is zero-distributed if and only if $Z_n = R_n + N_n$ with $\text{rank}(R_n)/d_n \to 0$ and $\|N_n\| \to 0$ as $n \to \infty$.*
- *$\{Z_n\}_n$ is zero-distributed if there exists a $p \in [1, \infty]$ such that $\|Z_n\|_p/(d_n)^{1/p} \to 0$ as $n \to \infty$.*

A.3 The ∗-algebra of block GLT sequences

Let $r \geq 1$ be a fixed positive integer. A r-block GLT sequence (or simply a GLT sequence if r can be inferred from the context or we do not need/want to specify it) is a special r-block matrix-sequence $\{A_n\}_n$ equipped with a measurable function $\kappa : [0, 1] \times [-\pi, \pi] \to \mathbb{C}^{r\times r}$, the so-called symbol or GLT symbol. We use the notation $\{A_n\}_n \sim_{\text{GLT}} \kappa$ to indicate that $\{A_n\}_n$ is a GLT sequence with symbol κ. The symbol of a GLT sequence is unique in the sense that if $\{A_n\}_n \sim_{\text{GLT}} \kappa$ and $\{A_n\}_n \sim_{\text{GLT}} \varsigma$ then $\kappa = \varsigma$ a.e. in the definition domain $[0, 1] \times [-\pi, \pi]$.

The main properties of r-block GLT sequences proved in [14] are listed [14, Chapter 5, pp. 85-86]: they represent a complete characterization of GLT sequences, equivalent to the full constructive definition given originally in [60] for $r = 1$ (see also the seminal paper by Tilli [65] for a previous less general construction). The power of r-block GLT sequence relies on the fact that they form a maximal ∗-algebra closed under algebraic operations, under mild assumption regarding only (psudo)-inversion. The algebraic structure carries over the related GLT symbols which allows to study in a compact way the eigenvalue and singular value distribution in the sense of Definition 2 with $t = 2$ of quite involved matrix-sequences.

Acknowledgements The work of all authors is supported by the Italian Agency INδAM-GNCS. The work of Ludovico Bruni Bruno is funded by INδAM and supported by Padova University. This author expresses

his gratitude to Insubria University, Junior Postdoc project 2022-2023 leaded by Matteo Semplice, on whose framework the majority of this research has been developed. Furthermore, Stefano Serra-Capizzano is grateful for the support of the Laboratory of Theory, Economics and Systems – Department of Computer Science at Athens University of Economics and Business.

Funding The work of all authors is supported by the Italian Agency INδAM-GNCS. The work of Ludovico Bruni Bruno is funded by INδAM and supported by Padova University. The work of Stefano Serra-Capizzano is funded from the European High-Performance Computing Joint Undertaking (JU) under grant agreement No 955701. The JU receives support from the European Union's Horizon 2020 research and innovation programme and Belgium, France, Germany, Switzerland.

Data Availability The data used for this article has been described in the paper. Otherwise missing data is available upon request.

Declarations

Conflicts of Interest The authors declare that they have no conflict of interest.

References

1. Abraham, R., Marsden, J.E., Ratiu, T.: Manifolds, tensor analysis, and applications. Applied Mathematical Sciences, vol. 75, 2nd edn. Springer-Verlag, New York (1988)
2. Ainsworth, M., Coyle, J.: Conditioning of hierarchic p-version Nédélec elements on meshes of curvilinear quadrilaterals and hexahedra. SIAM J. Numer. Anal. **41**, 731–750 (2003)
3. Alonso Rodríguez, A., Bruni Bruno, L., Rapetti, F.: Computing weights for high order Whitney edge elements. Dolomites Research Notes on Approximation **15**, 1–12 (2022)
4. Alonso Rodríguez, A., Bruni Bruno, L., Rapetti, F.: Towards nonuniform distributions of unisolvent weights for high-order Whitney edge elements. Calcolo **59**(37), 29 (2022)
5. Alonso Rodríguez, A., Bruni Bruno, L., Rapetti, F.: Flexible Weights for High Order Face Based Finite Element Interpolation, in Spectral and High Order Methods for Partial Differential Equations ICOSAHOM 2020+1, vol. 137 of Lect. Notes Comput. Sci. Eng., Springer, Cham, (2023), 117–128
6. Alonso Rodríguez, A., Bruni Bruno, L., Rapetti, F.: Whitney edge elements and the Runge phenomenon. J. Comput. Appl. Math. **427**(115117), 9 (2023)
7. Alonso Rodríguez, A., Camaño, J., De Los Santos, E., Rapetti, F.: Weights for moments' geometrical localization: a canonical isomorphism, Adv. Comput. Math., 50 , v86, 34 (2024)
8. Alonso Rodríguez, A., Rapetti, F.: On a generalization of the Lebesgue's constant. Journal of Computational Physics **428**, 109964 (2021)
9. Alonso Rodríguez, A., Rapetti, F., Zappon, E.: New degrees of freedom for high-order Whitney approximations of Darcy's flows. Numer. Algorithms **87**, 1613–1634 (2021)
10. Arnold, D.N., Falk, R.S., Winther, R.: Finite element exterior calculus, homological techniques, and applications. Acta Numer **15**, 1–155 (2006)
11. Arnold, D.N., Logg, A.: Periodic table of the finite elements, SIAM News, 47 (2014). Available at: http://femtable.org
12. Barbarino, G.: A systematic approach to reduced glt. BIT **62**, 681–743 (2022)
13. Barbarino, G., Garoni, C., Serra-Capizzano, S.: Block generalized locally toeplitz sequences: theory and applications in the multidimensional case. Electron. Trans. Numer. Anal. **53**, 113–216 (2020)

14. Barbarino, G., Garoni, C., Serra-Capizzano, S.: Block generalized locally toeplitz sequences: theory and applications in the unidimensional case. Electron. Trans. Numer. Anal. **53**, 28–112 (2020)
15. Beckermann, B., Kuijlaars, A.B.J.: Superlinear convergence of conjugate gradients. SIAM J. Numer. Anal. **39**, 300–329 (2001)
16. Beckermann, B., Serra-Capizzano, S.: On the asymptotic spectrum of finite element matrix sequences. SIAM J. Numer. Anal. **45**, 746–769 (2007)
17. Benzi, M., Olshanskii, M.A.: Field-of-values convergence analysis of augmented Lagrangian preconditioners for the linearized Navier-Stokes problem. SIAM J. Numer. Anal. **49**, 770–788 (2011)
18. Bhatia, R.: Matrix analysis. Graduate Texts in Mathematics, vol. 169. Springer-Verlag, New York (1997)
19. Bossavit, A.: Computational electromagnetism, Electromagnetism, Academic Press, Inc., San Diego, CA, (1998). Variational formulations, complementarity, edge elements
20. Bruni Bruno, L.: Weights as degrees of freedoom for high order Whitney finite elements, PhD thesis, University of Trento, (2022). Available at: https://theses.hal.science/tel-04067201/
21. Bruni Bruno, L., De Marchi, S., Elefante, G.: Polynomial approximation from diffused data: unisolvence and stablity, preprint, (2024). Available at: arXiv:2509.15813
22. Bruni Bruno, L., Erb, W.: Polynomial interpolation of function averages on interval segments, SIAM. J. Numer. Anal. **62**, 1759–1781 (2024)
23. Bruni Bruno, L., Erb, W.: The Fekete problem in segmental polynomial interpolation, BIT, 65 (2025), 3
24. Bruni Bruno, L., Zampa, E.: Unisolvent and minimal physical degrees of freedom for the second family of polynomial differential forms, ESAIM Math. Model. Numer. Anal. **56**, 2239–2253 (2022)
25. Castillo, P., Cockburn, B., Perugia, I., Schötzau, D.: An a priori error analysis of the local discontinuous Galerkin method for elliptic problems. SIAM J. Numer. Anal. **38**, 1676–1706 (2000)
26. Christiansen, S.H., Rapetti, F.: On high order finite element spaces of differential forms. Math. Comp. **85**, 517–548 (2016)
27. Ciarlet, P.G.: The finite element method for elliptic problems. Studies in Mathematics and its Applications, vol. 4. North-Holland Publishing Co., Amsterdam-New York-Oxford (1978)
28. Desbrun, M., Hirani, A.N., Leok, M., Marsden, J.E.: Discrete exterior calculus, 2005. Available at: https://arxiv.org/abs/math/0508341
29. Donatelli, M., Garoni, C., Manni, C., Serra-Capizzano, S., Speleers, H.: Robust and optimal multi-iterative techniques for IgA collocation linear systems. Comput. Methods Appl. Mech. Engrg. **284**, 1120–1146 (2015)
30. Donatelli, M., Garoni, C., Manni, C., Serra-Capizzano, S., Speleers, H.: Robust and optimal multi-iterative techniques for IgA Galerkin linear systems. Comput. Methods Appl. Mech. Engrg. **284**, 230–264 (2015)
31. Ern, A., Guermond, J.-L.: Finite Elements I: Interpolation and approximation, **72** of Texts in Applied Mathematics, Springer Cham, (2021)
32. Fekete, M.: Über die Verteilung der Wurzeln bei gewissen algebraischen Gleichungen mit ganzzahligen Koeffizienten. Math. Z. **17**, 228–249 (1923)
33. Garoni, C., Serra-Capizzano, S.: Generalized locally Toeplitz sequences: theory and applications, vol. I. Springer, Cham (2018)
34. Garoni, C., Serra-Capizzano, S.: Generalized locally Toeplitz sequences: theory and applications, vol. II. Springer, Cham (2018)
35. Garoni, C., Serra-Capizzano, S., Sesana, D.: Spectral analysis and spectral symbol of d-variate $\mathbb{Q}_p$ Lagrangian FEM stiffness matrices. SIAM J. Matrix Anal. Appl. **36**, 1100–1128 (2015)
36. Garoni, C., Speleers, H., Ekström, S.-E., Reali, A., Serra-Capizzano, S., Hughes, T.J.R.: Symbol-based analysis of finite element and isogeometric B-spline discretizations of eigenvalue problems: exposition and review. Arch. Comput. Methods Eng. **26**, 1639–1690 (2019)
37. Gerritsma, M.: Edge functions for spectral element methods, in Spectral and high order methods for partial differential equations, of Lect. Notes Comput. Sci. Eng., Springer, Heidelberg, **76**, 199–207 (2011)
38. Golinskii, L., Serra-Capizzano, S.: The asymptotic properties of the spectrum of nonsymmetrically perturbed Jacobi matrix sequences. J. Approx. Theory **144**, 84–102 (2007)
39. Golub, G.H., Van Loan, C.F.: Matrix computations, Johns Hopkins Studies in the Mathematical Sciences, Johns Hopkins University Press, Baltimore, MD, fourth ed., (2013)

40. Greenbaum, A., Pták, V., Strakoš, Z.: Any nonincreasing convergence curve is possible for GMRES. SIAM J. Matrix Anal. Appl. **17**, 465–469 (1996)
41. Hiptmair, R.: Canonical construction of finite elements. Math. Comp. **68**, 1325–1346 (1999)
42. Kuijlaars, A.B.J.: Convergence analysis of Krylov subspace iterations with methods from potential theory. SIAM Rev. **48**, 3–40 (2006)
43. Lee, J.M.: Introduction to smooth manifolds, vol. 218 of Graduate Texts in Mathematics, Springer, second ed., (2012)
44. Licht, M.W.: On basis constructions in finite element exterior calculus, Adv. Comput. Math., 48 (2022), 14, 36
45. Liesen, J., Strakoš, Z.: GMRES convergence analysis for a convection-diffusion model problem. SIAM J. Sci. Comput. **26**, 1989–2009 (2005)
46. Mazza, M., Ratnani, A., Serra-Capizzano, S.: Spectral analysis and spectral symbol for the 2D curl-curl (stabilized) operator with applications to the related iterative solutions. Math. Comp. **88**, 1155–1188 (2019)
47. Michel, S., Torlo, D., Ricchiuto, M., Abgrall, R.: Spectral analysis of continuous FEM for hyperbolic PDEs: influence of approximation, stabilization, and time-stepping. J. Sci. Comput. **89**(31), 41 (2021)
48. Michel, S., Torlo, D., Ricchiuto, M., Abgrall, R.: Spectral analysis of high order continuous FEM for hyperbolic PDEs on triangular meshes: influence of approximation, stabilization, and time-stepping. J. Sci. Comput. **94**(49), 48 (2023)
49. Nédélec, J.-C.: Mixed finite elements in R^3. Numer. Math. **35**, 315–341 (1980)
50. Nédélec, J.-C.: A new family of mixed finite elements in R^3. Numer. Math. **50**, 57–81 (1986)
51. Ng, M.K.: Iterative methods for Toeplitz systems. Oxford University Press, New York, Numerical Mathematics and Scientific Computation (2004)
52. Rahla, R.I., Serra-Capizzano, S., Tablino-Possio, C.: Spectral analysis of $\mathbb{P}_k$ finite element matrices in the case of Friedrichs-Keller triangulations via generalized locally Toeplitz technology, Numer. Linear Algebra Appl., 27, e2302, 28 (2020)
53. Rapetti, F.: High order edge elements on simplicial meshes. ESAIM Math. Model. Numer. Anal. **41**, 1001–1020 (2007)
54. Rapetti, F., Bossavit, A.: Whitney forms of higher degree. SIAM J. Numer. Anal. **47**, 2369–2386 (2009)
55. Robidoux, N.: Polynomial histopolation, superconvergent degrees of freedom, and pseudospectral discrete hodge operators, tech. rep., (2006)
56. Schwarz, G.: Hodge decomposition–a method for solving boundary value problems. Lecture Notes in Mathematics, vol. 1607. Springer-Verlag, Berlin (1995)
57. Serra, S.: Asymptotic results on the spectra of block Toeplitz preconditioned matrices. SIAM J. Matrix Anal. Appl. **20**, 31–44 (1999)
58. Serra-Capizzano, S.: Spectral behavior of matrix sequences and discretized boundary value problems. Linear Algebra Appl. **337**, 37–78 (2001)
59. Serra-Capizzano, S.: Matrix algebra preconditioners for multilevel Toeplitz matrices are not superlinear, Linear Algebra Appl., 343/344 (2002), 303–319. Special issue on structured and infinite systems of linear equations
60. Serra-Capizzano, S.: Generalized locally Toeplitz sequences: spectral analysis and applications to discretized partial differential equations, **366**, 2003, 371–402. Special issue on structured matrices: analysis, algorithms and applications (Cortona, 2000)
61. Serra-Capizzano, S.: An elementary proof of the exponential conditioning of real vandermonde matrices, Boll. Unione Mat. Ital. Sez. B Artic. Ric. Mat., 8:10, 761–768 (2010)
62. Serra-Capizzano, S., Tyrtyshnikov, E.: Any circulant-like preconditioner for multilevel matrices is not superlinear. SIAM J. Matrix Anal. Appl. **21**, 431–439 (1999)
63. Serra-Capizzano, S., Tyrtyshnikov, E.: How to prove that a preconditioner cannot be superlinear. Math. Comp. **72**, 1305–1316 (2003)
64. Shen, Z., Serkh, K.: On polynomial interpolation in the monomial basis. SIAM J. Numer. Anal. **63**, 469–494 (2025)
65. Tilli, P.: Locally Toeplitz sequences: spectral properties and applications. Linear Algebra Appl. **278**, 91–120 (1998)
66. Tilli, P.: A note on the spectral distribution of Toeplitz matrices, Linear Multilin. Algebra **45**, 147–159 (1998)
67. Tyrtyshnikov, E.E.: A unifying approach to some old and new theorems on distribution and clustering. Linear Algebra Appl. **232**, 1–43 (1996)

68. Warner, F.W.: Foundations of Differentiable Manifolds and Lie Groups, vol. 94 of Graduate Texts in Mathematics, Springer-Verlag, (1983)
69. Wendland, H.: On the convergence of a general class of finite volume methods. SIAM J. Numer. Anal. **43**, 987–1002 (2005)